Published OnlineFirst August 15, 2014; DOI: 10.1158/2326-6066.CIR-14-0098

26. Dighe AS, Richards E, Old LJ, Schreiber RD. Enhanced *in vivo* growth and resistance to rejection of tumor cells expressing dominant negative IFN gamma receptors. Immunity 1994;1:447–56.
27. Ranganath S, Ouyang W, Bhattarcharya D, Sha WC, Grupe A, Peltz G, et al. GATA-3-dependent enhancer activity in IL-4 gene regulation. J Immunol 1998;161:3822–6.
28. Hosoi A, Matsushita H, Shimizu K, Fujii SI, Ueha S, Abe J, et al. Adoptive cytotoxic T lymphocyte therapy triggers a counter-regulatory immunosuppressive mechanism via recruitment of myeloid-derived suppressor cells. Int J Cancer 2014;134:1810–22.
29. Hobeika AC, Etienne W, Torres BA, Johnson HM, Subramaniam PS. IFN-gamma induction of p21(WAF1) is required for cell cycle inhibition and suppression of apoptosis. J Interferon Cytokine Res 1999;19:1351–61.
30. Gooch JL, Herrera RE, Yee D. The role of p21 in interferon gamma-mediated growth inhibition of human breast cancer cells. Cell Growth Differ 2000;11:335–42.
31. Harvat BL, Seth P, Jetten AM. The role of p27Kip1 in gamma interferon-mediated growth arrest of mammary epithelial cells and related defects in mammary carcinoma cells. Oncogene 1997;14:2111–22.
32. Lee SH, Kim JW, Oh SH, Kim YJ, Rho SB, Park K, et al. IFN-gamma/IRF-1-induced p27kip1 down-regulates telomerase activity and human telomerase reverse transcriptase expression in human cervical cancer. FEBS Lett 2005;579:1027–33.
33. Dimco G, Knight RA, Latchman DS, Stephanou A. STAT1 interacts directly with cyclin D1/Cdk4 and mediates cell cycle arrest. Cell Cycle 2010;9:4638–49.
34. Melnikova VO, Bolshakov SV, Walker C, Ananthaswamy HN. Genomic alterations in spontaneous and carcinogen-induced murine melanoma cell lines. Oncogene 2004;23:2347–56.
35. Lin HK, Chen Z, Wang G, Nardella C, Lee SW, Chan CH, et al. Skp2 targeting suppresses tumorigenesis by Arf-p53-independent cellular senescence. Nature 2010;464:374–9.
36. Wang S, Raven JF, Koromilas AE. STAT1 represses Skp2 gene transcription to promote p27Kip1 stabilization in Ras-transformed cells. Mol Cancer Res 2010;8:798–805.
37. Delia D, Fontanella E, Ferrario C, Chessa L, Mizutani S. DNA damage-induced cell-cycle phase regulation of p53 and p21waf1 in normal and ATM-defective cells. Oncogene 2003;22:7866–9.
38. Kitagawa R, Kastan MB. The ATM-dependent DNA damage signaling pathway. Cold Spring Harb Symp Quant Biol 2005;70:99–109.
39. Perret R, Ronchese F. Effector CD8+ T cells activated *in vitro* confer immediate and long-term tumor protection *in vivo*. Eur J Immunol 2008;38:2886–95.
40. Imai N, Ikeda H, Tawara I, Shiku H. Tumor progression inhibits the induction of multifunctionality in adoptively transferred tumor-specific CD8+ T cells. Eur J Immunol 2009;39:241–53.
41. Kaplan DH, Shankaran V, Dighe AS, Stockert E, Aguet M, Old LJ, et al. Demonstration of an interferon gamma-dependent tumor surveillance system in immunocompetent mice. Proc Natl Acad Sci U S A 1998;95:7556–61.
42. Shankaran V, Ikeda H, Bruce AT, White JM, Swanson PE, Old LJ, et al. IFNgamma and lymphocytes prevent primary tumour development and shape tumour immunogenicity. Nature 2001;410:1107–11.
43. Koebel CM, Vermi W, Swann JB, Zerafa N, Rodig SJ, Old LJ, et al. Adaptive immunity maintains occult cancer in an equilibrium state. Nature 2007;450:903–7.
44. Schreiber RD, Old LJ, Smyth MJ. Cancer immunoediting: integrating immunity's roles in cancer suppression and promotion. Science 2011;331:1565–70.

Published OnlineFirst August 15, 2014; DOI: 10.1158/2326-6066.CIR-14-0098

AACR American Association for Cancer Research

Cancer Immunology Research

Cytotoxic T Lymphocytes Block Tumor Growth Both by Lytic Activity and IFN γ-Dependent Cell-Cycle Arrest

Hirokazu Matsushita, Akihiro Hosoi, Satoshi Ueha, et al.

Cancer Immunol Res 2015;3:26-36. Published OnlineFirst August 15, 2014.

Published OnlineFirst February 20, 2015; DOI: 10.1158/2326-6066.CIR-14-0190

Research Article

Cancer Immunology Research

Robust Antitumor Effects of Combined Anti-CD4-Depleting Antibody and Anti-PD-1/PD-L1 Immune Checkpoint Antibody Treatment in Mice

Satoshi Ueha[1], Shoji Yokochi[1,2], Yoshiro Ishiwata[1,2], Haru Ogiwara[1], Krishant Chand[1], Takuya Nakajima[1], Kosuke Hachiga[1,2], Shigeyuki Shichino[1], Yuya Terashima[1], Etsuko Toda[1], Francis H.W. Shand[3], Kazuhiro Kakimi[4], Satoru Ito[1,2], and Kouji Matsushima[1]

Abstract

Depletion of $CD4^+$ cells in tumor-bearing mice has strong antitumor effects. However, the mechanisms underlying these effects and the therapeutic benefits of $CD4^+$ cell depletion relative to other immunotherapies have not been fully evaluated. Here, we investigated the antitumor effects of an anti-CD4-depleting mAb as a monotherapy or in combination with immune checkpoint mAbs. In B16F10, Colon 26, or Lewis lung carcinoma subcutaneous tumor models, administration of the anti-CD4 mAb alone had strong antitumor effects that were superior to those elicited by $CD25^+$ Treg depletion or other immune checkpoint mAbs, and which were completely reversed by $CD8^+$ cell depletion. $CD4^+$ cell depletion led to the proliferation of tumor-specific $CD8^+$ T cells in the draining lymph node and increased infiltration of PD-1^+CD8^+ T cells into the tumor, with a shift toward type I immunity within the tumor. Combination treatment with the anti-CD4 mAb and immune checkpoint mAbs, particularly anti-PD-1 or anti-PD-L1 mAbs, synergistically suppressed tumor growth and greatly prolonged survival. To our knowledge, this work represents the first report of robust synergy between anti-CD4 and anti-PD-1 or anti-PD-L1 mAb therapies. *Cancer Immunol Res; 3(6); 1–10.* ©2015 AACR.

Introduction

Immune checkpoint modulators such as those targeting cytotoxic T-lymphocyte–associated antigen-4 (CTLA-4) and programmed cell death-1 (PD-1) have attracted attention due to their extraordinary antitumor effects in patients with advanced melanoma, lung cancer, and renal cancer (1, 2). An mAb against CTLA-4 (ipilimumab) that enhances both early T-cell activation and CTL function was approved for treatment of patients with advanced melanoma in the United States in 2011. An anti–PD-1 mAb (nivolumab) that protects activated T cells from exhaustion in peripheral tissues was approved for treatment of patients with melanoma in Japan and in the United States in 2014. In addition, other mAbs against CTLA-4 (tremelimumab), PD-1 (pembrolizumab), and programmed death-ligand 1 (PD-L1, a ligand for PD-1) are currently undergoing clinical trials to evaluate their antitumor efficacy. However, despite clear survival benefits in a subset of tumor patients, other groups of patients are refractory to these single-agent therapies.

Combination therapies comprising immune checkpoint modulators that have different points of action, targeting, for example, the activation and expansion of T cells in lymphoid tissues and the exhaustion and deletion of T cells in the effector site, represent promising strategies for tumor immunotherapy (1). Synergistic antitumor effects in advanced melanoma have been reported with a combination of anti–CTLA-4 and anti–PD-1 mAbs (3). The antitumor efficacy of other combinations of regulators of lymphocyte activation and expansion (e.g., Lymphocyte activation gene-3/LAG-3, OX40/CD134) and of lymphocyte exhaustion and deletion (e.g., T-cell immunoglobulin mucin-3/TIM-3, 4-1BB/CD137, B- and T-lymphocyte attenuator/BTLA, glucocorticoid-induced TNF-receptor/GITR) is currently under investigation. Because immune checkpoint modulators play both positive and negative roles in the immune inhibitory pathway with some redundancy, identification of optimal therapeutic combinations remains a considerable challenge.

Another approach to immune checkpoint modulation involves depleting immunosuppressive leukocyte populations such as forkhead box P3 (Foxp3)$^+$$CD25^+$ regulatory T cells (Treg), Th2 cells, T regulatory (Tr) 1/3 cells (4), myeloid-derived suppressor cells (MDSC) and indoleamine-2,3-dioxygenase (IDO)$^+$ plasmacytoid DCs (pDC; refs. 5–7). Several groups have suggested that depletion of $CD4^+$ cells, including Tregs, Th2 cells, Tr1/3 cells, and a subpopulation of MDSCs and pDCs, results in strong antitumor effects in mouse models due to the enhancement of CTL responses (8–12). These antitumor effects may be associated with the modulation of multiple immune checkpoints caused by

[1]Department of Molecular Preventive Medicine, Graduate School of Medicine, The University of Tokyo, Tokyo, Japan. [2]IDAC Theranostics, Inc., Tokyo, Japan. [3]Department of Pharmacology and Therapeutics, The University of Melbourne, Melbourne, Victoria, Australia. [4]Department of Immunotherapeutics, The University of Tokyo Hospital, Tokyo, Japan.

Note: Supplementary data for this article are available at Cancer Immunology Research Online (http://cancerimmunolres.aacrjournals.org/).

S. Ueha, S. Yokochi, and Y. Ishiwata contributed equally to this article.

Corresponding Author: Kouji Matsushima, The University of Tokyo, 7-3-1 Hongo, Bunkyo-ku, Tokyo 1130033, Japan. Phone: 81-3-5841-3431; Fax: 81-3-5684-2297; E-mail: koujim@m.u-tokyo.ac.jp

doi: 10.1158/2326-6066.CIR-14-0190

Published OnlineFirst February 20, 2015; DOI: 10.1158/2326-6066.CIR-14-0190

$CD4^+$ cell depletion. However, the relative advantage of $CD4^+$ cell depletion over other immune checkpoint mAb-based treatments remains unclear. Encouraged by the positive reports surrounding the benefits of anti-CD4 mAb treatment in mice, and by the recent clinical data supporting anti–CTLA-4 and anti–PD-1 mAb therapies, here, we examine whether treatments that combine an anti-CD4 mAb and immune checkpoint modulators produce synergistic antitumor activity.

Thus, in the present study, we used comprehensive immunologic analyses to compare the antitumor effects of an anti–CD4-depleting mAb with those of a variety of mAbs against immune checkpoint molecules, including PD-1, PD-L1, PD-L2, CTLA-4, OX40, LAG-3, TIM-3, BTLA, and GITR, in mouse subcutaneous tumor models. We also investigated the antitumor effects of treatments that combined an anti-CD4 mAb and antibodies against these immune checkpoint molecules. We report that treatment with an anti-CD4 mAb alone induces strong antitumor effects and expansion of tumor-specific $CD8^+$ T cells, and that combination of an anti-CD4 mAb with anti–PD-1 or anti–PD-L1 mAbs results in striking synergy in the suppression of tumor growth.

Materials and Methods

Mouse

Seven-week-old female C57BL/6 and male BALB/c mice were purchased from Japan SLC. Fluorescent ubiquitination-based cell-cycle indicator (Fucci) double transgenic mice were generated by crossbreeding FucciG_1-#639 and FucciS/G_2/M-#474 animals (obtained from Dr. A. Miyawaki through the RIKEN BRC) as described previously (13). Mice transgenic for the gp100 melanoma antigen-specific Pmel-1-TCR or the ovalbumin-specific OT-I TCR were purchased from The Jackson Laboratory. Each experimental group contained 8 mice except where otherwise specified. All animal experiments were conducted in accordance with institutional guidelines with the approval of the Animal Care and Use Committee of the University of Tokyo.

Cell lines and tumor models

B16F10 and Lewis lung carcinoma (LLC) were obtained from the ATCC. Colon 26 was obtained from the Cell Resource Center for Biomedical Research, Institute of Development, Aging, and Cancer, Tohoku University. B16F10 cells expressing the truncated form of human low-affinity nerve growth factor receptor (ΔhLNGFR/hCD271) were generated by retroviral transduction and two subsequent rounds of *in vivo* passaging (Supplementary Fig. S1). B16F10 cells (5×10^5/mouse), LLC cells (5×10^5/mouse), and Colon 26 cells (2×10^5/mouse) were inoculated s.c. into the right flanks of C57BL/6 or BALB/c mice. Tumor diameter was measured twice weekly and used to calculate tumor volume (mm^3) [(major axis; mm) × (minor axis; $mm)^2 \times 0.5236$].

In vivo antibody treatment

Anti-CD4 (clone GK1.5), anti-CD8 (clone YTS169.4), anti–PD-1 (clone J43), anti–PD-L1 (clone 10F.9G2), anti–PD-L2 (clone TY25), anti-OX40 (clone OX-86), anti–CTLA-4 (clone 9D9), anti–LAG-3 (clone C9B7W), anti-BTLA (clone 6A6), anti–TIM-3 (clone RMT3-23), anti-GITR (clone DTA-1), and anti-CD25 (clone PC-61.5.3) mAbs were purchased from BioXcell. Antibodies were injected i.p. at a dose of 200 μg per mouse. Anti-CD4 mAb (200 μg/mouse) was administered in a single dose or in successive doses on days 5 and 9 after tumor inoculation. Immune checkpoint antibodies (200 μg/mouse) were administered on days 4, 8, 14, and 18 after tumor inoculation. Combination treatments with the anti-CD4 mAb and anti-immune checkpoint antibodies were administered under the same conditions as respective single-agent protocols.

Immunohistologic analysis

Immunofluorescent staining was performed as described previously (14–16) using primary antibodies and the appropriate fluorophore-conjugated secondary Abs as listed in Supplementary Table S1, then photographed using an SP5 confocal microscope (Leica Microsystems).

Flow cytometry

Intravascular leukocytes were stained by i.v. injection of fluorophore-conjugated mAb (3 μg/mouse) against CD45 or CD45.2 3 minutes before collecting tissues. Single-cell suspensions were prepared by enzymatic or mechanical dissociation of tissues with or without subsequent density separation, as described previously (17, 18). Flow-Count fluorospheres (Beckman Coulter) were used to determine cell numbers and normalize cell concentrations before antibody staining. Cells were pretreated with Fc Block (anti-mouse CD16/CD32 mAb; clone 2.4G2, BioXcell), then stained with mix of fluorophore-conjugated anti-mouse mAbs as indicated in Supplementary Table S1. Data were acquired on a Gallios flow cytometer (Beckman Coulter) and analyzed using FlowJo software (version 9.7.5; FlowJo, LLC). Nonviable cells were excluded from the analysis based on forward and side scatter profiles and propidium iodide staining.

Quantitative reverse transcription real-time PCR

Total RNA was extracted using a RNeasy Mini kit (Qiagen) and converted to cDNA using ReverTra Ace qPCR RT Master Mix with gDNA Remover (Toyobo) according to the manufacturer's instructions. Real-time quantitative PCR analysis was performed using THUNDERBIRD Probe qPCR Mix or THUNDERBIRD SYBR qPCR Mix (Toyobo), and an ABI 7500 sequence detector system (Life Technologies). The primers used for the PCR reaction are listed in Supplementary Table S2. The expression levels of each gene were normalized to *Rps3* expression level for each sample.

Statistical analysis

Unless otherwise stated, data are presented as mean ± SE. Statistical analyses were performed using GraphPad Prism software (version 6.0e; GraphPad Software). For comparisons between groups in the *in vivo* study, we used one-way ANOVA with the Dunnett *post hoc* test. For comparisons between the means of two variables, we used paired Student *t* tests. Comparisons of survival data between groups were made using the log-rank test after Kaplan–Meier analysis. A P value of <0.05 was considered to be statistically significant.

Results

An optimized anti-CD4 mAb treatment protocol exerts robust antitumor effects

We began by optimizing the protocol for anti-CD4 mAb administration in B16F10, LLC and Colon 26 tumor models. Mice bearing subcutaneous tumors received a single i.p. injection of 200 μg anti-CD4 mAb 2 days before (day −2) or 0, 3, 5, or

Published OnlineFirst February 20, 2015; DOI: 10.1158/2326-6066.CIR-14-0190

9 days after tumor inoculation. In all three models, administration of anti-CD4 mAb on days 3 and 5 significantly suppressed tumor growth (Supplementary Fig. S2A–S2C). B16F10 tumor growth, but not LLC and Colon 26 tumor growth, was also inhibited by mAb administration on days −2 and 0 (Supplementary Fig. S2A). However, the growth of LLC and Colon 26 tumors was not significantly affected by mAb administration at days −2 and 0 (Supplementary Fig. S2B and S2C). Successive administration of the anti-CD4 mAb on days 5 and 9 resulted in the greatest inhibition of tumor growth in all three models (data not shown). Doses of anti-CD4 mAb (3.1 or 12.5 μg/mouse) that were insufficient to cause CD4 lymphocyte depletion had no inhibitory effect on tumor growth in the melanoma model (Supplementary Fig. S2D and S2E). On the basis of these results, for subsequent studies, we adopted a protocol of administering the anti-CD4 mAb at a dose of 200 μg/mouse successively on days 5 and 9 after tumor inoculation.

We next compared the antitumor effects of the anti-CD4 mAb against those of a variety of immune checkpoint mAbs (PD-1, PD-L1, PD-L2, CTLA-4, OX40, LAG-3, TIM-3, BTLA, and GITR) in the B16F10 model, because melanoma is a major target of anti-immune checkpoint antibody therapy. We found that twice-weekly injections of immune checkpoint antibodies were sufficient to produce the same level of antitumor effect as achieved with daily injections (data not shown). Among the mAbs tested, the anti-CD4 mAb was the most effective single-agent treatment in terms of tumor growth inhibition and survival (Fig. 1A–C). Collectively, these results confirm the potent antitumor effects of anti-CD4 mAb treatment in mice and reveal a surprising advantage of anti-CD4 mAb treatment over immune checkpoint mAb treatment.

Anti-CD4 mAb treatment depletes CD4$^+$ T cells and pDCs

To determine which cells are depleted by anti-CD4 mAb therapy, we next examined changes in cell populations with immunosuppressive potential following anti-CD4 mAb administration at day 5 in mice bearing B16F10 tumors. Flow cytometric analysis revealed that numbers of CD4$^+$ T cells, including Foxp3$^+$ CD25$^+$ Tregs, decreased 50- to 100-fold over days 2 to 9 following anti-CD4 mAb administration (7 to 14 days after tumor inoculation), as compared with cell numbers in phase-matched untreated tumor-bearing mice (Supplementary Fig. S3A–S3C). When LLC tumor-bearing mice were administered anti-CD4 mAb on days 5 and 9, CD4$^+$ T cells disappeared from the blood until at least day 15 after the first mAb administration (Supplementary Fig. S3D). pDCs, a subset of which are positive for CD4 and have been implicated in the suppression of antitumor immune responses (7), also decreased 3- to 10-fold over days 2 to 9 following mAb treatment (Supplementary Fig. S3A–S3C). MDSC subpopulations, including neutrophils and Ly-6C^{hi} or Ly-6C^{lo} monocytes, were not significantly affected by mAb treatment (data not shown). These results indicate that CD4$^+$ T cells (including Tregs) and pDCs are the targets of anti-CD4 mAb therapy.

Anti-CD4 mAb treatment increases the number of tumor-infiltrating CD8$^+$ T cells

We next investigated the effects of anti-CD4 mAb therapy on tumor-infiltrating CD8$^+$ T-cell populations. Intravascular staining (IVS) is a technique that allows circulating leukocytes present in tissue blood vessels (which represent a proportion of total leukocytes recovered) to be distinguished from cells

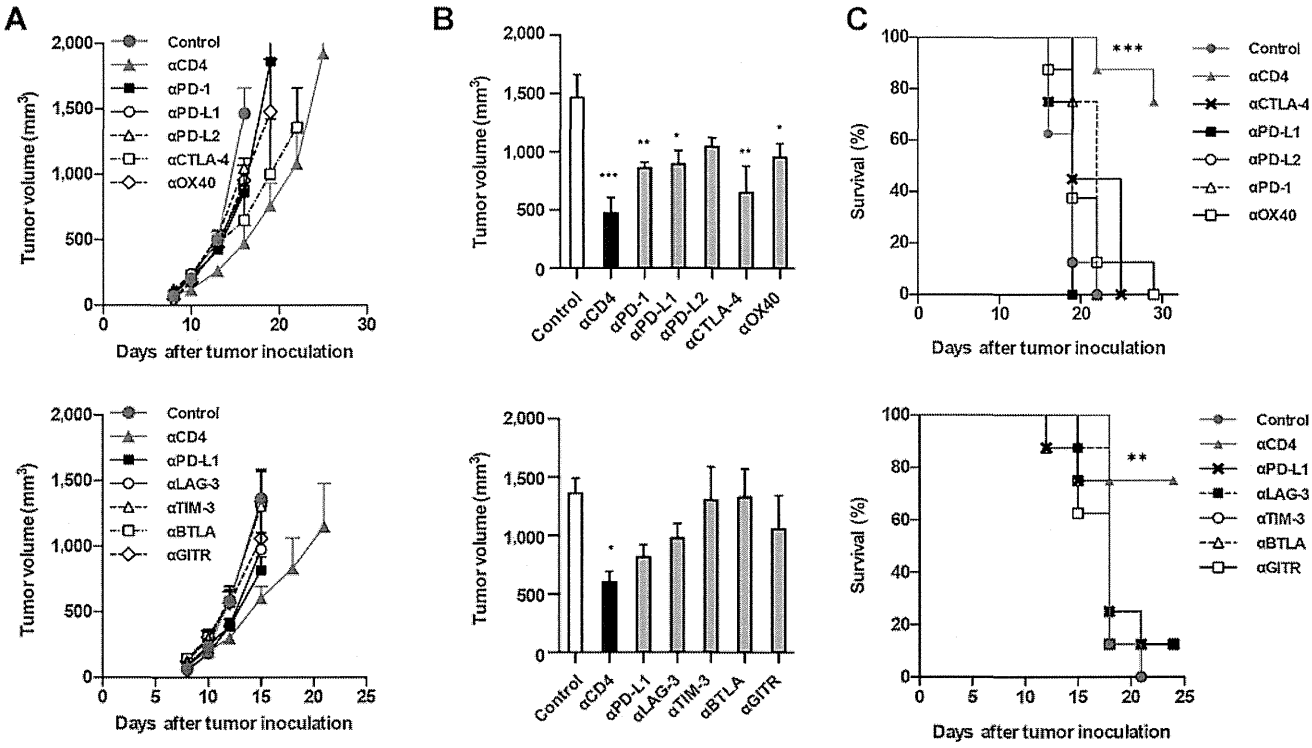

Figure 1.

Antitumor effects of anti-CD4 mAb treatment. Mice bearing B16F10 melanoma tumors were injected i.p. with anti-CD4 mAb (200 μg/mouse) on days 5 and 9 or anti-immune checkpoint mAbs on days 4, 8, 14, and 18 after tumor inoculation. A, tumor growth curves. B, tumor volume on day 16 (top) or day 15 (bottom). C, survival following tumor inoculation (8 mice/group). A and B, data, mean ± SE of 8 mice per group; *, $P < 0.05$; **, $P < 0.01$; ***, $P < 0.001$ (compared with control).

Published OnlineFirst February 20, 2015; DOI: 10.1158/2326-6066.CIR-14-0190

actually infiltrating the parenchyma of tissues, including tumors (19). In untreated B16F10 tumors, about 15% of $CD8^+$ T cells were positive for IVS, and the frequency of $PD\text{-}1^+CD137^+$ tumor-reactive cells (20) was about 10-fold lower in this population than in the IVS-negative parenchymal cell population (Supplementary Fig. S4A and S4B). Anti-CD4 mAb treatment significantly increased the frequency and number of IVS-$CD45^-CD8^+$ T cells in the tumor (Fig. 2A and B). The increased number of $CD8^+$ T cells in the tumors of anti-CD4 mAb-treated mice was also evident in histologic sections (Fig. 2C). Furthermore, the IVS-$CD8^+$ T cells induced by anti-CD4 mAb treatment contained a higher proportion of $PD\text{-}1^+CD137^+$ tumor-reactive cells (Fig. 2D and E), had greater potential to produce IFNγ in response to *ex vivo* PMA/ionomycin stimulation (Fig. 2F and G), and showed higher specific killing activity against B16F10 tumor cells (Supplementary Fig. S5A–S5C), compared with T cells from the untreated group. In the LLC and Colon 26 tumor models, anti-CD4 mAb-treated mice displayed decreased tumor growth, systemically increased $CD8^+CD44^{hi}PD\text{-}1^+$ T cells, and upregulation of LAG-3, TIM-3, and CTLA-4 in tumor-infiltrating $CD8^+$ T cells (Supplementary Fig. S6A–S6D). Collectively, these results suggest that anti-CD4 mAb treatment enhances antitumor $CD8^+$ T-cell responses and induces a shift toward type I immunity within the tumor.

Anti-CD4 mAb treatment promotes expansion of tumor-specific $CD8^+$ T cells in the draining lymph node

To further investigate the effects of anti-CD4 mAb treatment on tumor-specific $CD8^+$ T-cell responses, we adoptively transferred melanoma antigen-specific Pmel-1 TCR transgenic $CD8^+$ T cells (21) into mice 1 day before inoculation with B16F10 tumors (day −1; Supplementary Fig. S7A and S7B). On day 14 after tumor inoculation, numbers of Pmel-1 $CD8^+$ T cells in the blood, draining lymph node (dLN), non-dLN (ndLN), spleen and tumor were 10- to 100-fold higher in anti-CD4 mAb-treated mice compared with that in untreated mice (Supplementary Fig. S7C and S7D). As tumors grew, Pmel-1 $CD8^+$ T-cell numbers were unchanged or decreased in untreated group mice, whereas Pmel-1 $CD8^+$ T-cell numbers increased in anti-CD4 mAb-treated mice (Supplementary Fig. S7E). To determine the site of Pmel-1 $CD8^+$ T-cell expansion, we administered bromodeoxyuridine (BrdUrd) 1 hour before collecting tissues. The number of $BrdU^+$-proliferating Pmel-1 $CD8^+$ T cells in the dLN far outnumbered those in the tumor, irrespective of anti-CD4 mAb treatment (Supplementary Fig. S7F and S7G). Importantly, proliferating cell numbers decreased between days 9 and 14 in untreated mice, but increased in anti-CD4 mAb-treated mice (Supplementary Fig. S7H). Similar CD4 depletion–induced proliferation was also observed in endogenous polyclonal $CD8^+$ T cells (data not shown). These data suggest that anti-CD4 mAb treatment protects tumor-reactive

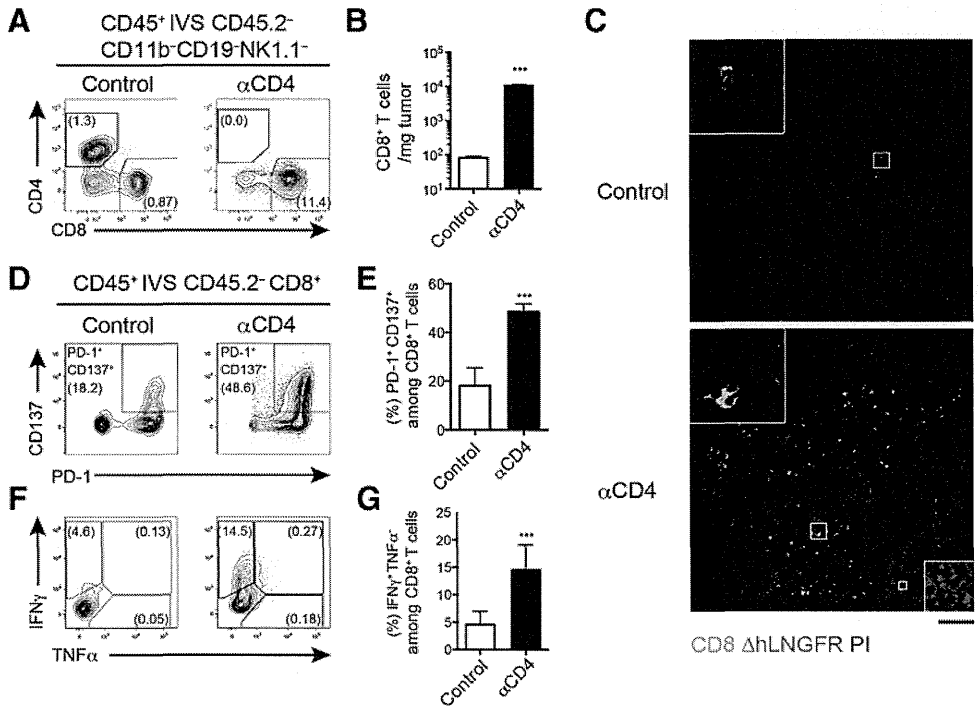

Figure 2.

Anti-CD4 mAb treatment increases the number of tumor-infiltrating $CD8^+$ T cells. Mice bearing B16F10 (A, B, D–G) or B16F10-ΔhLNGFR (C) tumors were injected i.p. with anti-CD4 mAb on days 5 and 9, and tumor-infiltrating $CD8^+$ T cells were analyzed on day 14 after tumor inoculation. Control mice received an injection of vehicle only. For flow cytometric analyses, mice were given an i.v. injection of anti-CD45.2 Ab 3 minutes before the collection of tissues to enable identification of cells in the blood compartment (IVS). A, flow-cytometry plots of parenchymal leukocyte compartments ($CD45^+$IVS-$CD45.2^-$). B, the number of parenchymal $CD8^+$ T cells in tumor. C, distribution of $CD8^+$ T cells in the tumor. Green, CD8; red, ΔhLNGFR; blue, propidium iodide (PI). Enlargements in white boxes show nonnecrotic areas, yellow box shows necrotic area; scale bar, 200 μm. D, flow-cytometry plots and frequencies (E) of $PD\text{-}1^+CD137^+$ tumor-reactive cells among the parenchymal $CD8^+$ T-cell population. F, flow-cytometry plots and frequencies (G) of IFNγ- and TNFα-producing cells among the parenchymal $CD8^+$ T-cell population following *ex vivo* restimulation with PMA and ionomycin. Data represent mean ± SE of 4 mice per group and are representative of at least four independent experiments. Numbers in flow-cytometry plots indicate mean frequencies within live cells (A) or parental populations (D and F); ***, $P < 0.001$ (compared with control).

Published OnlineFirst February 20, 2015; DOI: 10.1158/2326-6066.CIR-14-0190

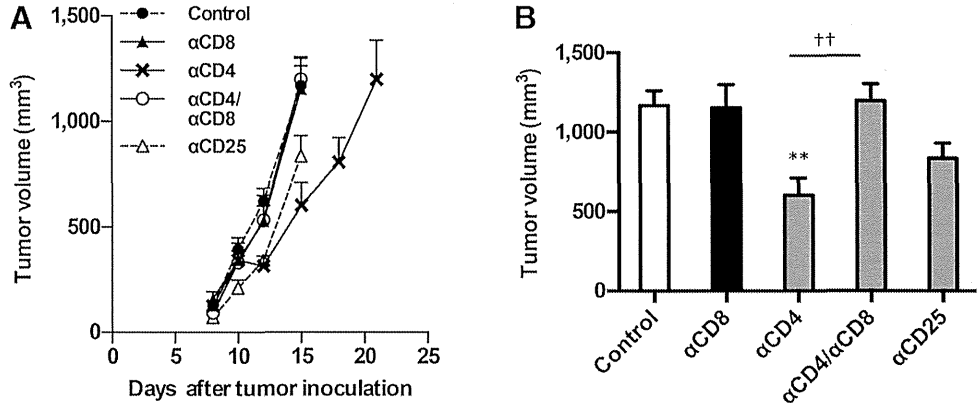

Figure 3.
CD8$^+$ T cells play a pivotal role in the antitumor effects of anti-CD4 mAb treatment. Mice bearing B16F10 tumors were injected i.p. with anti-CD4, anti-CD8, and/or anti-CD25 mAbs (200 μg/mouse) on days 5 and 9 after tumor inoculation. A, tumor growth curves. B, tumor volume on day 15 after tumor inoculation. Data, mean ± SE of 8 mice per group; **, $P < 0.05$ (compared with control); ††, $P < 0.01$ (comparison as indicated).

CD8$^+$ T cells from deletion, a mechanism of peripheral tolerance in which the continuous and excessive exposure of antigen-specific T cells to cognate antigens eventually results in the loss of the antigen-specific T-cell clones.

To confirm the effects of anti-CD4 mAb treatment on the proliferation of CD8$^+$ T cells, we used fluorescent ubiquitination-based cell-cycle indicator (Fucci) double transgenic mice. In Fucci mice, Fucci-orange (mKO2) and Fucci-green (mAG) are expressed reciprocally in the G_0–G_1 and S–G_2–M phases of the cell cycle, respectively (13, 18). In the B16F10 tumor model, anti-CD4 mAb treatment significantly increased the proportion of mAG$^+$ proliferating cells among CD8$^+$CD44^{hi} T cells in both the dLN and non-dLN, compared with the proportion of these cells in untreated control mice (Supplementary Fig. S7I and S7J).

To determine whether this CD4 depletion–induced proliferation was specific for tumor-specific CD8$^+$ T cells or was a tumor antigen-independent response such as homeostatic proliferation (22), we adoptively transferred a CFSE-labeled mixture of Pmel-1, ovalbumin-specific OT-I, and polyclonal CD8$^+$ T cells into B16 tumor-bearing or tumor-free mice with or without anti-CD4 mAb treatment (Supplementary Fig. S8A). Pmel-1, but not OT-I or polyclonal CD8$^+$ T cells, selectively proliferated in the dLN of B16 tumor-bearing mice (Supplementary Fig. S8B–S8E). These results indicate that CD4 depletion–induced T-cell expansion is specific for tumor-specific CD8$^+$ T cells. Collectively, these results suggest that anti-CD4 mAb treatment systemically increases the availability of tumor-specific CD8$^+$ T cells by enhancing their proliferation in the dLN in a tumor-associated antigen-dependent manner.

Enhanced CD8$^+$ T-cell responses underlie the antitumor effects of anti-CD4 mAb treatment

To determine whether enhanced CTL responses are responsible for the antitumor effects of anti-CD4 mAb treatment, we administered the anti-CD4 mAb together with an anti–CD8-depleting mAb. When the anti–CD8-depleting mAb was administered together with the anti-CD4 mAb, the inhibitory effect of anti-CD4 mAb treatment on tumor growth was completely reversed (Fig. 3A and B). We also investigated whether treatment with an anti–CD25-depleting mAb, which is widely used to deplete Foxp3$^+$CD25$^+$ Tregs in mice (23), could produce the same effect as anti-CD4 mAb treatment. Under our administration protocol, tumor growth in the anti-CD25 mAb-treated group was almost equivalent to that observed in untreated mice (Fig. 3A and B). These results suggest that the tumor-specific CD8$^+$ T cells that are induced by anti-CD4 mAb treatment are responsible for the antitumor effects of the treatment, and that anti-CD4 mAb treatment might deplete immunosuppressive populations more efficiently than anti-CD25 mAb treatment.

Combination treatment with anti-CD4 and anti–PD-1 or anti–PD-L1 mAbs synergistically enhances antitumor effects

Next, we examined whether synergistic antitumor effects could be achieved by supplementing anti-CD4 mAb treatment with various immune checkpoint mAbs, particularly those targeting the exhaustion and deletion phase of the immune response. We devised a combination treatment protocol of anti-CD4 mAb with immune checkpoint antibodies as depicted in Fig. 4A. Strikingly, combination treatment with anti-CD4 and anti–PD-L1 mAbs, and to a lesser extent anti-CD4 and anti–PD-1 mAbs, resulted in dramatic synergistic inhibition of tumor growth in the B16F10 melanoma model (Fig. 4B and C). Combination treatment with anti-CD4 and anti–CTLA-4, anti–TIM-3, anti-BTLA, and anti-GITR mAbs also had additive or synergistic effects (Fig. 4B and C), but anti–PD-L2, anti-OX40 and anti–LAG-3 mAbs produced no synergistic antitumor effect when combined with the anti-CD4 mAb (Fig. 4B and C). Survival was also prolonged by combination treatment with anti-CD4 and anti–PD-L1 mAbs compared with anti-CD4 mAb monotherapy, but not by other combinations of anti-CD4 and immune checkpoint mAbs (Fig. 4D). Importantly, depletion of CD8$^+$ T cells completely abrogated the tumor growth inhibition induced by the combination of anti-CD4 and anti–PD-1 or PD-L1 mAbs, indicating that CD8$^+$ T cells play a critical role in the antitumor effects of the combination treatment (Fig. 4E).

To determine whether the synergistic antitumor effects of anti-CD4 and anti–PD-1 or anti–PD-L1 mAb treatment are common to other tumor types and mouse strains, we examined the effect of combination treatment in the Colon 26 subcutaneous tumor model in BALB/c mice. The anti–PD-1 or anti–PD-L1 mAb treatment alone did not inhibit tumor growth, whereas combination treatment with anti-CD4 and anti–PD-1 or anti–PD-L1 mAbs resulted in strong synergistic inhibition of tumor growth (Fig. 5A and B). These effects were completely reversed by treatment with an anti–CD8-depleting mAb (Fig. 5B). Notably, we observed complete remission in 3 of 10 mice treated with the anti-CD4/anti–PD-1 mAb combination, and in 6 of 10 mice treated with the anti-CD4/anti–PD-L1 mAb combination. In addition, the 6 mice that rejected the tumor in the anti-CD4/anti–PD-L1 mAb-treated group were resistant to rechallenge with Colon 26 tumor cells at a dose five times higher than that used in the initial inoculation (Fig. 5C). Collectively, these results indicate that combination

Published OnlineFirst February 20, 2015; DOI: 10.1158/2326-6066.CIR-14-0190

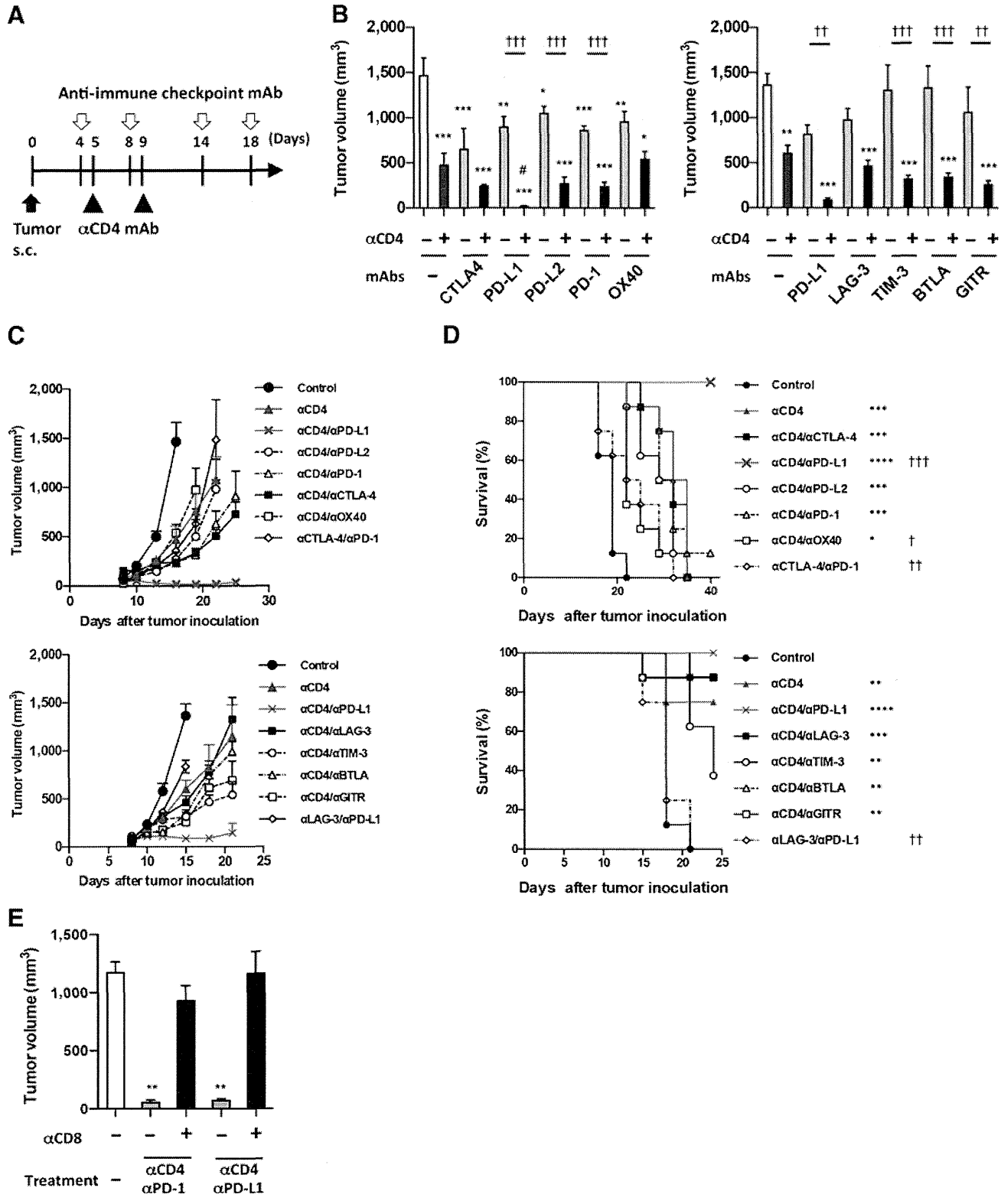

Figure 4.
Combination treatment with anti-CD4 and anti–PD-1 or anti–PD-L1 mAbs has synergistic antitumor effects. Mice bearing B16F10 tumors received anti-CD4 mAb, anti-immune checkpoint mAb, or a combination of these, according to the treatment schedule shown in A. B, tumor volume on day 16 (left) or 15 (right); *, $P < 0.05$; **, $P < 0.01$; ***, $P < 0.001$ (compared with control); #, $P = 0.021$ (compared with αCD4); ††, $P < 0.01$; †††, $P < 0.001$ (comparisons as indicated). C, tumor growth curves. D, survival plots representative of two independent experiments; *, $P < 0.05$; **, $P < 0.01$; ***, $P < 0.001$; ****, $P < 0.0001$ (compared with control); †, $P < 0.05$; ††, $P < 0.01$; †††, $P < 0.001$ (compared with αCD4). E, anti-CD8 mAb was administered together with anti-CD4 mAb and tumor volumes were measured on day 16; **, $P < 0.01$ (compared with control). Data, mean ± SE of 8 mice per group.

Published OnlineFirst February 20, 2015; DOI: 10.1158/2326-6066.CIR-14-0190

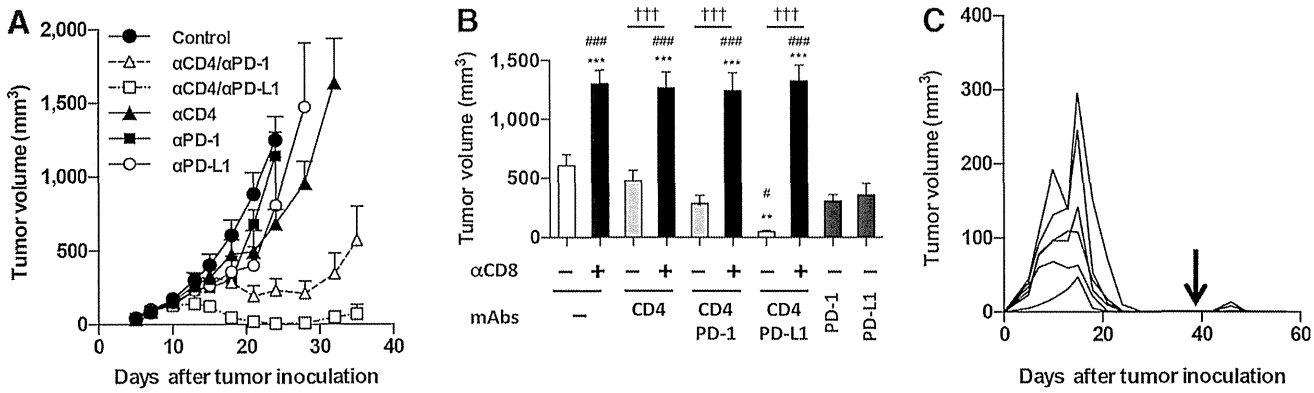

Figure 5.

Combination treatment with anti-CD4 and anti–PD-1 or anti–PD-L1 mAbs induces long-term antitumor $CD8^+$ T-cell memory. Mice bearing Colon 26 tumors received anti-CD4, anti–PD-L1, anti–PD-1 or anti-CD8 mAbs or a combination of these according to the treatment schedule shown in Fig. 4A. A, tumor growth curves. B, tumor volume on day 18; **, $P < 0.01$; ***, $P < 0.001$ (compared with control); #, $P = 0.029$; ###, $P < 0.001$ (compared with αCD4); †††, $P < 0.001$ (comparisons as indicated). C, the 6 mice that achieved complete remission of Colon 26 tumors after anti-CD4 and anti–PD-L1 treatment were rechallenged on day 39 with Colon 26 tumor cells at five times the cell number of the initial challenge. Arrow indicates day of rechallenge; *, $P < 0.05$; **, $P < 0.01$ (compared with control). A and B, data, mean ± SE of 10 mice per group.

treatment with anti-CD4 and anti–PD-1 or anti–PD-L1 mAbs has a dramatic and robust antitumor effect that is mediated by antitumor $CD8^+$ T cells.

Blockade of the PD-1/PD-L1 signaling axis increases the number of PD-1^+ tumor-reactive $CD8^+$ T cells in the circulation

Finally, we investigated the cellular and molecular mechanisms underlying the synergy between anti-CD4 and anti–PD-1 or anti–PD-L1 mAbs in the B16F10 melanoma model. Quantitative RT-PCR analysis of whole tumor tissue demonstrated that anti-CD4 mAb treatment alone augmented expression of the antitumor cytokine genes *Ifng* and *Tnf*, the IFNγ-inducible genes *Cxcl10* and *Cd274*/PD-L1 (24, 25), and genes encoding the proapoptotic molecules *Fasl*, *Prf1*/perforin, and *Gzmb*/Granzyme B, compared with the expression levels of these genes in untreated tumors (Supplementary Fig. S9A and S9B). The upregulation of PD-L1 by anti-CD4 mAb treatment was also observed at the protein level (Supplementary Fig. S9C). However, no additive or synergistic effects on gene expression were observed in groups receiving combination treatment with anti-CD4 and anti–PD-1 or PD-L1 mAbs. Consistent with these results, the proportion of IFNγ-producing and TNFα-producing cells within the tumor-infiltrating $CD8^+$ T-cell population was equivalent between mice receiving anti-CD4 mAb alone and mice receiving the combination of anti-CD4 and anti–PD-1 or anti–PD-L1 mAbs (data not shown).

We next analyzed the effects of anti–PD-1 and anti–PD-L1 mAbs on the PD-1^+CD8^+ T cells that increased in number in the systemic circulation in response to anti-CD4 mAb treatment. We examined cell populations expressing the effector/memory T-cell marker CD44 and the activation marker CD137. Combination treatment with anti-CD4 and anti–PD-L1 mAbs increased the frequency of $CD44^{hi}$PD-1^+ cells among $CD8^+$ T cells in the blood, dLN and non-dLN, compared with that in mice receiving the anti-CD4 mAb alone (blood data shown in Fig. 6A and B). In blood $CD8^+$ T cells, expression levels of PD-1 on cells within the $CD44^{hi}$ PD-1^+ population and the frequency of PD-1^+CD137^+ cells were significantly higher in mice that received the combination of anti-CD4 and anti–PD-L1 mAbs compared with the corresponding expression levels and frequency in mice that received the anti-CD4 mAb alone (Fig. 6A–C). In contrast, combination treatment with anti-CD4 and anti–PD-1 mAbs decreased the frequency of the $CD44^{hi}$PD-1^+ population among blood $CD8^+$ T cells, and decreased the expression levels of PD-1 on cells within the $CD44^{hi}$ PD-1^+ population (Fig. 6A, E, and F). However, the frequency of the $CD44^{hi}CD137^+$ tumor-reactive cell population was higher in mice receiving the combination of anti-CD4 and anti–PD-1 mAbs compared with mice receiving the anti-CD4 mAb alone (Fig. 6A, E, and F), suggesting that anti–PD-1 mAb treatment does not actually decrease the number of tumor-reactive $CD8^+$ T cells in the blood, but rather decreases the level of PD-1 expression on these cells. On the other hand, the frequency of PD-1^+ cells among tumor-infiltrating $CD8^+$ T cells in anti-CD4 mAb-treated mice was not affected by treatment with anti–PD-1 or anti–PD-L1 mAbs (Fig. 6D and G).

Discussion

The recent success of anti–CTLA-4 and anti–PD-1 mAb therapies in the clinic has highlighted the potential of immunotherapy for the treatment of cancer (2, 3, 26–29). However, the development of immunotherapy for widespread clinical use remains in its early stages. Extensive efforts have been directed toward enhancing endogenous antitumor immunity by dampening the influence of immunosuppressive mechanisms. Treatment strategies have included combinations of antibodies with other antibodies and with other immunotherapies or anticancer therapeutics. In the present study, we demonstrate that antibody-mediated depletion of $CD4^+$ cells from tumor-bearing mice results in enhanced polyclonal PD-1^+CD137^+ tumor-reactive and monoclonal tumor-specific Pmel-1 $CD8^+$ T-cell responses, and strong inhibition of tumor growth. Combination treatment with the anti-CD4 mAb and various immune checkpoint mAbs, particularly anti–PD-1 and anti–PD-L1 mAbs, revealed striking synergy in suppressing tumor growth and prolonging survival.

Several previous reports have described antitumor activity of anti-CD4 mAb treatment in solid tumor models in C57BL/6 mice, including subcutaneous tumors induced by inoculation with B16 melanoma cells (9, 11, 12), recurrent TC1 lung cancer cells (30), or embryo cells expressing the adenovirus-derived E1A protein (10). Although the efficacy of immunotherapy in mouse tumor

Published OnlineFirst February 20, 2015; DOI: 10.1158/2326-6066.CIR-14-0190

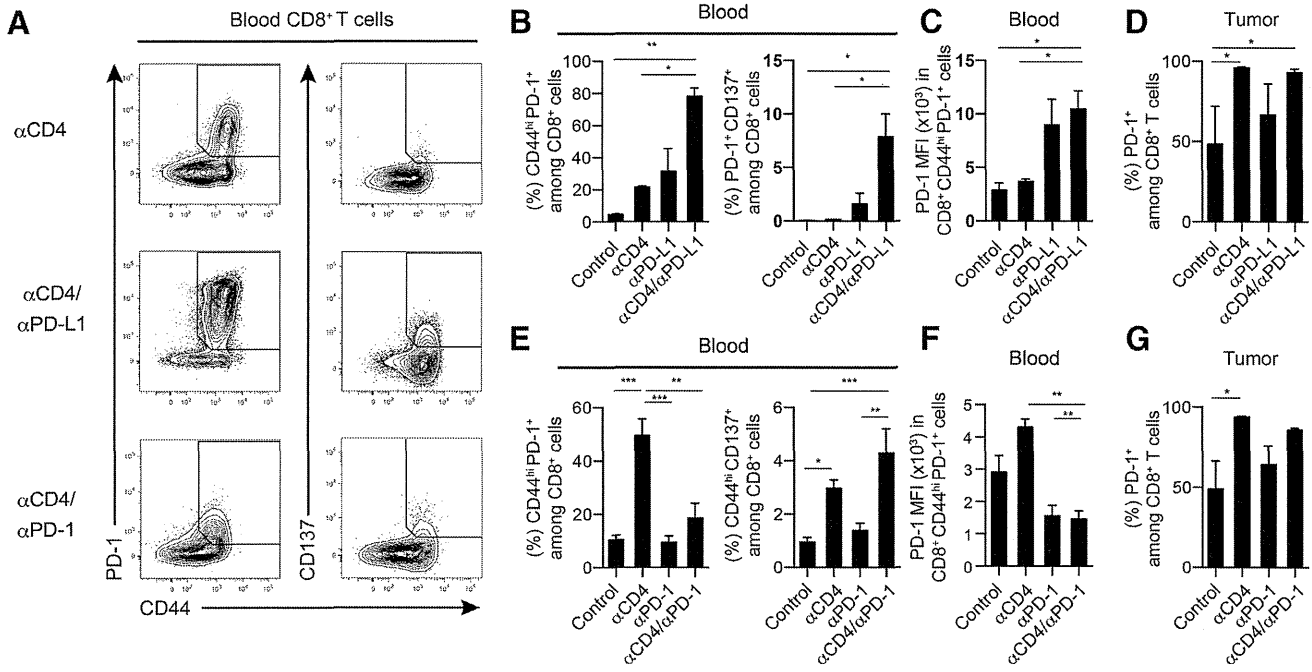

Figure 6.

Anti-PD-L1 and anti-PD-1 treatments target PD-1$^+$CD8$^+$ T cells that are induced by anti-CD4 treatment. Mice bearing B16F10 tumors were treated with anti-CD4, anti-PD-L1, or anti-PD-1 mAbs, or a combination of these according to the treatment schedule shown in Fig. 4A. A, flow-cytometry plots of blood CD8$^+$ T cells. B and E, proportions of CD44^{hi} PD-1$^+$ cells, PD-1$^+$CD137$^+$ cells or CD44^{hi}CD137$^+$ cells among blood CD8$^+$ T cells on day 14. C and F, mean fluorescent intensity (MFI) of PD-1 expression on CD8$^+$CD44^{hi}PD-1$^+$ cells in the blood. D and G, proportions of PD-1$^+$ cells among tumor-infiltrating CD8$^+$ T cells. B–D, show anti-PD-L1 mAb experiments; E to G, show anti-PD-1 mAb experiments. Data, mean ± SE of 4 mice per group and are representative of two independent experiments; *, $P < 0.05$; **, $P < 0.01$; ***, $P < 0.001$.

models often depends on tumor type, taken together, these reports from independent groups and our results from the present study suggest that anti-CD4 mAb treatment is likely to have broad-spectrum antitumor activity against solid tumors. Optimization of the anti-CD4 mAb administration protocol revealed robust antitumor effects when mice received the mAb on days 3 or 5, rather than when mice receive the mAb before tumor inoculation (day −2). These results suggest that pretreatment is not necessary. However, priming and/or the preexistence of activated CD8$^+$ T cells are important for effective anti-CD4 mAb therapy. Although the mechanistic link between the timing of anti-CD4 antibody administration and the efficacy of treatment remains to be elucidated, administration of the antibody to patients with early-stage cancer or whose tumor burden has been reduced by surgical resection, irradiation or chemotherapeutics is likely to be most beneficial.

A dose of anti-CD4 mAb sufficient to deplete most CD4$^+$ cells was required in order for antitumor effects to be observed. The CD4$^+$ cell population includes Foxp3$^+$CD25$^+$ Tregs, Th2 cells, Tr1/3 cells (4), and IDO$^+$ immunosuppressive pDCs (7). Considering that markedly increased proliferation of tumor-specific CD8$^+$ T cells was observed in the dLN, anti-CD4 mAb treatment is likely to augment proliferation of tumor-reactive CD8$^+$ T cells through the removal of these CD4$^+$ immunosuppressive cells from the dLN. In addition, anti-CD4 mAb treatment increased the proportion of PD-1$^+$CD137$^+$ tumor-reactive cells and IFNγ-producing cells among tumor-infiltrating CD8$^+$ T cells in the B16F10 model, suggesting that anti-CD4 mAb treatment augmented both the quantity and quality of tumor-specific CD8$^+$ T-cell responses. We recently demonstrated that IFNγ- and TNFα-induced cell-cycle arrest is an important mechanism underlying the antitumor effects induced by tumor-specific CD8$^+$ T-cell transfer (31). The shift toward IFNγ-dominant type I immunity, which was evident in the strong induction of IFNγ and TNFα in tumor-infiltrating CD8$^+$ T cells after anti-CD4 mAb treatment, is likely to play a central role in the antitumor effects that we observed (32). Notably, depletion of CD25$^+$ Tregs by administration of an anti-CD25 mAb on days 5 and 9 after tumor inoculation did not reproduce the antitumor effect of anti-CD4 mAb treatment. Because some Foxp3$^+$ Tregs have low-to-negative CD25 expression, residual Foxp3$^+$CD25$^{-/lo}$ Tregs may have contributed to this discrepancy. Moreover, the antitumor effects of anti-CD25 mAb treatment have been reported to be optimal when the mAb is administered before tumor inoculation (33, 34), because when it is administered after tumor inoculation, the anti-CD25 mAb depletes not only Tregs but also other activated lymphocytes expressing CD25. The involvement of Treg and other CD4$^+$-immunosuppressive populations in the suppression of CD8$^+$ T-cell–mediated antitumor responses remains to be elucidated.

The synergy that occurs in combination treatment with anti-CD4 and anti–PD-1 or anti–PD-L1 mAbs is likely due to the blockade of PD-1/PD-L1 signaling in PD-1$^+$ activated CD8$^+$ T cells that are induced by anti-CD4 mAb treatment. We did not detect any synergistic effect in terms of the quantity and quality of the tumor-infiltrating CD8$^+$ T-cell response promoted by anti-CD4 and anti–PD-1 or anti–PD-L1 mAb treatment. However, the frequency of the PD-1$^+$CD137$^+$ and CD44^{hi}CD137$^+$ tumor-reactive populations increased among CD8$^+$ T cells in the blood upon blockade of the PD-1/PD-L1 signaling axis. Considering

Published OnlineFirst February 20, 2015; DOI: 10.1158/2326-6066.CIR-14-0190

that T cells continuously traffic between peripheral and secondary lymphoid tissues via the lymph–blood circulation, the blockade of PD-1/PD-L1 signaling may prevent exhaustion or deletion of tumor-reactive PD-1$^+$CD8$^+$ T cells in the tumor and allow them to migrate into the dLN, thus sustaining antitumor CD8$^+$ T-cell responses. In addition, anti-CD4 mAb treatment increased the number of IFNγ-producing PD-1$^+$CD8$^+$ T cells in the tumor, resulting in the upregulation of IFNγ-inducible genes, including PD-L1. Although the shift toward IFNγ-dominant type-I immunity within the tumor contributes to the inhibition of tumor growth, it also promotes the exhaustion or deletion of tumor-infiltrating PD-1$^+$CD8$^+$ T cells by enhancing PD-1/PD-L1 signaling. It is therefore likely that the synergy of the anti-CD4 and anti–PD-1 or anti–PD-L1 mAb combination treatment arises due to the blockade of this adverse negative feedback mechanism.

We are in the process of developing a humanized anti-CD4 mAb with potent antibody-dependent cell-mediated cytotoxicity as an anticancer therapeutic. Because CD4$^+$ T cells play important roles in both humoral and cellular immunity, the heightened risk of infectious diseases that may be associated with transient CD4$^+$ T-cell depletion should be carefully evaluated in clinical trials. In addition, trials should seek to maximize clinical efficacy and safety through rigorous optimization of the antibody administration protocol. In preclinical studies in nonhuman primates, no serious adverse effects were detected after several weeks of treatment with our humanized anti-human CD4 mAb that resulted in CD4$^+$ T-cell depletion. In addition, no severe adverse effects have been observed during phase II clinical trials for T-cell malignancy with long-term administration of other humanized anti-CD4 mAbs (35, 36). Preexisting humoral immune mediators, such as immunoglobulin, plasma cells, and memory B cells, CD8$^+$ T-cell responses, and unimpaired natural immunity, are likely to provide basal protection against infectious diseases during CD4$^+$ T-cell–depleting therapies. On the other hand, consideration should also be given to the potential for the acute exacerbation of chronic diseases associated with viral infection (e.g., hepatitis C and B) due to excessive activation of effector and memory CD8$^+$ T cells after CD4$^+$ cell depletion.

In conclusion, our study represents the first report of robust antitumor effects of combination treatment with an anti–CD4-depleting antibody and anti–PD-1 or anti–PD-L1 immune checkpoint antibodies in mice. We have also characterized the immunologic bases for the synergy between these agents. Recent clinical trials suggest that anti–PD-1, anti–PD-L1, or anti–CTLA-4 mAbs, or combinations of these agents, are not effective against all types of solid tumors. Our findings suggest that combination treatment with an anti-CD4 mAb and immune checkpoint mAbs, particularly anti–PD-1 or anti–PD-L1 mAbs, is likely to result in greater clinical efficacy against a broader range of cancers.

Disclosure of Potential Conflicts of Interest

S. Ueha has ownership interest (including patents) in IDAC Theranostics. S. Yokochi is a manager at IDAC Theranostics. K. Hachiga is a researcher at IDAC Theranostics. K. Matsushima reports receiving a commercial research grant, has ownership interest (including patents), and is a consultant/advisory board member for IDAC Theranostics, Inc. No potential conflicts of interest were disclosed by the other authors.

Authors' Contributions

Conception and design: S. Ueha, S. Yokochi, Y. Ishiwata, S. Ito, K. Matsushima
Development of methodology: S. Ueha, S. Yokochi, Y. Ishiwata
Acquisition of data (provided animals, acquired and managed patients, provided facilities, etc.): S. Ueha, S. Yokochi, Y. Ishiwata, H. Ogiwara, K. Chand, K. Hachiga, Y. Terashima, E. Toda, K. Kakimi
Analysis and interpretation of data (e.g., statistical analysis, biostatistics, computational analysis): S. Ueha, S. Yokochi, Y. Ishiwata, K. Chand, T. Nakajima, K. Hachiga, S. Shichino, S. Ito, K. Matsushima
Writing, review, and/or revision of the manuscript: S. Ueha, S. Yokochi, S. Shichino, F.H.W. Shand, S. Ito, K. Matsushima
Administrative, technical, or material support (i.e., reporting or organizing data, constructing databases): S. Ueha, S. Yokochi, H. Ogiwara, S. Shichino
Study supervision: S. Ueha, K. Matsushima

Acknowledgments

The authors thank A. Miyawaki, A. Sakaue-Sawano, and the RIKEN BioResource Center for providing FucciG1 and FucciS/G2/M mice; A. Hosoi for assistance with Pmel-1-B16F10 experiments; H. Yamazaki, K. Tsuji, and K. Yoshioka for animal care; A. Yamashita, S. Aoki, and S. Fujita for expert technical assistance; and M. Otsuji, K. Takeda, and S. Shibayama for helpful discussions.

Grant Support

This work was supported by the Japan Science and Technology Agency CREST program; Grants-in-Aid for Scientific Research (C) 25460491 (to S. Ueha) and (B) 25293113 (to K. Matsushima) from the Japanese Ministry of Education, Culture, Sports, Science and Technology; and Health and Labor Science Research Grants for Research for Promotion of Cancer Control (Applied Research for Innovative Treatment of Cancer).

The costs of publication of this article were defrayed in part by the payment of page charges. This article must therefore be hereby marked *advertisement* in accordance with 18 U.S.C. Section 1734 solely to indicate this fact.

Received October 8, 2014; revised February 1, 2015; accepted February 15, 2015; published OnlineFirst February 20, 2015.

References

1. Pardoll DM. The blockade of immune checkpoints in cancer immunotherapy. Nat Rev Cancer 2012;12:252–64.
2. Topalian SL, Weiner GJ, Pardoll DM. Cancer immunotherapy comes of age. J Clin Oncol 2011;29:4828–36.
3. Wolchok JD, Kluger H, Callahan MK, Postow MA, Rizvi NA, Lesokhin AM, et al. Nivolumab plus ipilimumab in advanced melanoma. N Engl J Med 2013;369:122–33.
4. Whiteside TL. Disarming suppressor cells to improve immunotherapy. Cancer Immunol Immunother 2012;61:283–8.
5. Alizadeh D, Larmonier N. Chemotherapeutic targeting of cancer-induced immunosuppressive cells. Cancer Res 2014;74:2663–8.
6. Camisaschi C, De Filippo A, Beretta V, Vergani B, Villa A, Vergani E, et al. Alternative activation of human plasmacytoid DCs *in vitro* and in melanoma lesions: involvement of LAG-3. J Invest Dermatol 2014;134:1893–902.
7. Matta BM, Castellaneta A, Thomson AW. Tolerogenic plasmacytoid DC. European J Immunol 2010;40:2667–76.
8. Nagai H, Hara I, Horikawa T, Fujii M, Kurimoto M, Kamidono S, et al. Antitumor effects on mouse melanoma elicited by local secretion of interleukin-12 and their enhancement by treatment with interleukin-18. Cancer Invest 2000;18:206–13.
9. Nagai H, Hara I, Horikawa T, Oka M, Kamidono S, Ichihashi M. Elimination of CD4(+) T cells enhances anti-tumor effect of locally secreted interleukin-12 on B16 mouse melanoma and induces vitiligo-like coat color alteration. J Invest Dermatol 2000;115:1059–64.

Published OnlineFirst February 20, 2015; DOI: 10.1158/2326-6066.CIR-14-0190

10. den Boer AT, van Mierlo GJ, Fransen MF, Melief CJ, Offringa R, Toes RE. CD4+ T cells are able to promote tumor growth through inhibition of tumor-specific $CD8^+$ T-cell responses in tumor-bearing hosts. Cancer Res 2005;65:6984–9.
11. Yu P, Lee Y, Liu W, Krausz T, Chong A, Schreiber H, et al. Intratumor depletion of $CD4^+$ cells unmasks tumor immunogenicity leading to the rejection of late-stage tumors. J Exp Med 2005;201:779–91.
12. Choi BK, Kim YH, Kang WJ, Lee SK, Kim KH, Shin SM, et al. Mechanisms involved in synergistic anticancer immunity of anti-4–1BB and anti-CD4 therapy. Cancer Res 2007;67:8891–9.
13. Sakaue-Sawano A, Kurokawa H, Morimura T, Hanyu A, Hama H, Osawa H, et al. Visualizing spatiotemporal dynamics of multicellular cell-cycle progression. Cell 2008;132:487–98.
14. Ueha S, Yoneyama H, Hontsu S, Kurachi M, Kitabatake M, Abe J, et al. CCR7 mediates the migration of $Foxp3^+$ regulatory T cells to the paracortical areas of peripheral lymph nodes through high endothelial venules. J Leukoc Biol 2007;82:1230–8.
15. Ueha S, Murai M, Yoneyama H, Kitabatake M, Imai T, Shimaoka T, et al. Intervention of MAdCAM-1 or fractalkine alleviates graft-versus-host reaction associated intestinal injury while preserving graft-versus-tumor effects. J Leukoc Biol 2007;81:176–85.
16. Shono Y, Ueha S, Wang Y, Abe J, Kurachi M, Matsuno Y, et al. Bone marrow graft-versus-host disease: early destruction of hematopoietic niche after MHC-mismatched hematopoietic stem cell transplantation. Blood 2010; 115:5401–11.
17. Sawanobori Y, Ueha S, Kurachi M, Shimaoka T, Talmadge JE, Abe J, et al. Chemokine-mediated rapid turnover of myeloid-derived suppressor cells in tumor-bearing mice. Blood 2008;111:5457–66.
18. Shand FH, Ueha S, Otsuji M, Koid SS, Shichino S, Tsukui T, et al. Tracking of intertissue migration reveals the origins of tumor-infiltrating monocytes. ProcNatl Acad Sci U S A 2014;111:7771–6.
19. Anderson KG, Mayer-Barber K, Sung H, Beura L, James BR, Taylor JJ, et al. Intravascular staining for discrimination of vascular and tissue leukocytes. Nat Protoc 2014;9:209–22.
20. Ye Q, Song DG, Poussin M, Yamamoto T, Best A, Li C, et al. CD137 accurately identifies and enriches for naturally occurring tumor-reactive T cells in tumor. Clin Cancer Res 2014;20:44–55.
21. Overwijk WW, Theoret MR, Finkelstein SE, Surman DR, de Jong LA, Vyth-Dreese FA, et al. Tumor regression and autoimmunity after reversal of a functionally tolerant state of self-reactive $CD8^+$ T cells. J Exp Med 2003;198:569–80.
22. Surh CD, Sprent J. Homeostasis of naive and memory T cells. Immunity 2008;29:848–62.
23. Sakaguchi S. Regulatory T cells: history and perspective. Methods Mol Biol 2011;707:3–17.
24. Dong H, Strome SE, Salomao DR, Tamura H, Hirano F, Flies DB, et al. Tumor-associated B7-H1 promotes T-cell apoptosis: a potential mechanism of immune evasion. Nature Med 2002;8:793–800.
25. Furuta J, Inozume T, Harada K, Shimada S. CD271 on melanoma cell is an IFN-gamma-inducible immunosuppressive factor that mediates downregulation of melanoma antigens. J Invest Dermatol 2014;134: 1369–77.
26. Couzin-Frankel J. Breakthrough of the year 2013. Cancer immunotherapy. Science 2013;342:1432–3.
27. Hamid O, Robert C, Daud A, Hodi FS, Hwu WJ, Kefford R, et al. Safety and tumor responses with lambrolizumab (anti-PD-1) in melanoma. N Engl J Med 2013;369:134–44.
28. Topalian SL, Drake CG, Pardoll DM. Targeting the PD-1/B7-H1(PD-L1) pathway to activate anti-tumor immunity. Curr Opin Immunol 2012; 24:207–12.
29. Topalian SL, Hodi FS, Brahmer JR, Gettinger SN, Smith DC, McDermott DF, et al. Safety, activity, and immune correlates of anti-PD-1 antibody in cancer. N Engl J Med 2012;366:2443–54.
30. Predina J, Eruslanov E, Judy B, Kapoor V, Cheng G, Wang LC, et al. Changes in the local tumor microenvironment in recurrent cancers may explain the failure of vaccines after surgery. Proc Natl Acad Sci U S A 2013;110: E415–24.
31. Matsushita H, Hosoi A, Ueha S, Abe J, Fujieda N, Tomura M, et al. Cytotoxic T lymphocytes block tumor growth both by lytic activity and IFN-gamma-dependent cell-cycle arrest. Cancer Immunol Res 2015;3:26–36.
32. Braumuller H, Wieder T, Brenner E, Assmann S, Hahn M, Alkhaled M, et al. T-helper-1-cell cytokines drive cancer into senescence. Nature 2013;494: 361–5.
33. Onizuka S, Tawara I, Shimizu J, Sakaguchi S, Fujita T, Nakayama E. Tumor rejection by *in vivo* administration of anti-CD25 (interleukin-2 receptor alpha) monoclonal antibody. Cancer Res 1999;59:3128–33.
34. Shimizu J, Yamazaki S, Sakaguchi S. Induction of tumor immunity by removing $CD25^+CD4^+$ T cells: a common basis between tumor immunity and autoimmunity. J Immunol 1999;163:5211–8.
35. Kim YH, Duvic M, Obitz E, Gniadecki R, Iversen L, Osterborg A, et al. Clinical efficacy of zanolimumab (HuMax-CD4): two phase 2 studies in refractory cutaneous T-cell lymphoma. Blood 2007;109:4655–62.
36. Rider DA, Havenith CE, de Ridder R, Schuurman J, Favre C, Cooper JC, et al. A human CD4 monoclonal antibody for the treatment of T-cell lymphoma combines inhibition of T-cell signaling by a dual mechanism with potent Fc-dependent effector activity. Cancer Res 2007;67:9945–53.

Published OnlineFirst February 20, 2015; DOI: 10.1158/2326-6066.CIR-14-0190

AACR American Association for Cancer Research

Cancer Immunology Research

Robust Antitumor Effects of Combined Anti–CD4-Depleting Antibody and Anti–PD-1/PD-L1 Immune Checkpoint Antibody Treatment in Mice

Satoshi Ueha, Shoji Yokochi, Yoshiro Ishiwata, et al.

Cancer Immunol Res Published OnlineFirst February 20, 2015.

Increase in Activated Treg in TIL in Lung Cancer and In Vitro Depletion of Treg by ADCC Using an Antihuman CCR4 mAb (KM2760)

Koji Kurose, MD, Yoshihiro Ohue, MD, PhD,* Eiichi Sato, MD, PhD,† Akira Yamauchi, MD, PhD,‡ Shingo Eikawa, PhD,§ Midori Isobe, PhD,* Yumi Nishio, MS,* Akiko Uenaka, PhD,‖ Mikio Oka, MD, PhD,* and Eiichi Nakayama, MD, PhD‖*

Introduction: Tregs infiltrate tumors and inhibit immune responses against them.

Methods: We investigated subpopulations of Foxp3$^+$ CD4 T cells previously defined by Miyara et al. (*Immunity* 30, 899–911, 2009) in peripheral blood mononuclear cells (PBMCs) and tumor infiltrating lymphocytes (TILs) in lung cancer. We also showed that Tregs in healthy donors that express CCR4 could be efficiently eliminated in vitro by cotreatment with antihuman (h) CCR4 mAb (KM2760) and NK cells.

Results: In lung cancer, the number of activated/effector Tregs and non-Tregs, but not resting/naive Tregs, was increased in TILs compared with the number of those cells in PBMCs. The non-Treg population contained Th2 and Th17. CCR4 expression on activated/effector Tregs and non-Tregs in TILs was down-regulated compared with that on those cells in PBMCs. Chemokinetic migration of CD25$^+$ CD4 T cells containing the Treg population sorted from the PBMCs of healthy donors to CCL22/MDC was abrogated by pretreatment with anti-hCCR4 mAb (KM2760). The inhibitory activity of CD25$^+$ CD127$^{dim/-}$ CD4 Tregs on the proliferative response of CD4 and CD8 T cells stimulated with anti-CD3/CD28 coated beads was abrogated by adding an anti-hCCR4 mAb (KM2760) and CD56$^+$ NK cells to the culture.

Conclusions: The findings suggested the CCR4 on activated/effector Tregs and non-Tregs was functionally involved in the chemokinetic migration and accumulation of those cells to the tumor site. In vitro findings of efficient elimination of Tregs may give the basis for implementation of a clinical trial to investigate Treg depletion by administration of an anti-hCCR4 mAb to solid cancer patients.

Key Words: Lung cancer, Tregs, CCR4, Anti-hCCR4 mAb, Treg depletion.

(*J Thorac Oncol.* 2015;10: 74–83)

Infiltration of Tregs to local tumor sites has been shown in various murine and human tumors.[1] Tregs inhibit immune responses against tumors and also diminish the immunotherapeutic effects which activate host immune responses.[2,3] The CD8 T cells to Tregs ratio correlated with a favorable prognosis in some human cancers.[4,5] Tregs appeared to inhibit the priming of CD8 and also CD4 T cells by preventing the maturation of dendritic cells in tumor-draining lymph nodes.[6] Depletion of Tregs facilitated the induction of antitumor responses.[7] Two main populations of Foxp3$^+$ Tregs have been identified: a "naturally occurring" (n) Treg which differentiates within the thymus during T-cell ontogenesis and an "induced" (i) Treg which develops in the periphery from conventional CD4 T cells.[8] Conversion of CD4 T cells into iTregs occurs via various mechanisms involving the exposure to transforming growth factor beta (TGFβ) and other inhibitory cytokines, interleukin (IL)-6 or IL-10, and the interaction with dendritic cells.[9]

The accumulation of Tregs is mainly due to chemokine gradients. Chemokine receptors such as CCR4, CCR5, CCR6, CCR7, and CCR8 are responsible for Treg migration to tumor tissues, and also inflammatory sites and lymph nodes in response to various CC chemokines.[10] Of those, Tregs preferentially express CCR4 as compared with conventional T cells.[11] Moreover, CCR4-expressing Tregs represent active Tregs with strong inhibitory activity. The involvement of CCR4- and CCR4-associated chemokines, CCL17/TARC and CCL22/MDC, in Treg migration have been documented.[12,13] Tumor cells or intratumor myeloid cells produce CCL17/TARC and CCL 22/MDC.

Foxp3 is a key transcription factor for CD4 Tregs.[14] Miyara et al.[15] reported that human Foxp3$^+$ CD4 T cells were composed of three functionally and phenotypically distinct

*Department of Respiratory Medicine, Kawasaki Medical School, Kurashiki, Japan; †Department of Pathology, Tokyo Medical University, Tokyo, Japan; ‡Department of Biochemistry, Kawasaki Medical School, Kurashiki, Japan; §Department of Immunology, Okayama University Graduate School of Medicine, Dentistry and Pharmaceutical Sciences, Okayama, Japan; and ‖Faculty of Health and Welfare, Kawasaki University of Medical Welfare, Kurashiki, Japan.

Disclosure: This study was supported by the P-DIRECT, Ministry of Education, Culture, Sports, Science and Technology of Japan to Eiichi Nakayama, by a grant from the Ministry of Health, Labour and Welfare of Japan to Eiichi Nakayama and Mikio Oka, by JSPS KAKENHI (23591169 to Mikio Oka and 25430161 to Eiichi Nakayama), by a Research Project Grant from Kawasaki Medical School to Koji Kurose, by a grant from Kawasaki University of Medical Welfare to Eiichi Nakayama and by a grant from Kyowa Hakko Kirin to Eiichi Nakayama.

Address for correspondence: Eiichi Nakayama, MD, PhD, Faculty of Health and Welfare, Kawasaki University of Medical Welfare, 288 Matsushima, Kurashiki, Okayama 701-0193, Japan. E-mail: nakayama@mw.kawasaki-m.ac.jp

DOI: 10.1097/JTO.0000000000000364

ISSN: 1556-0864/15/1001-0074

subpopulations.[15] CD45RA$^+$ Foxp3^{lo} resting/naive Tregs and CD45RA$^-$ Foxp3^{hi} activated/effector Tregs were suppressive, whereas a CD45RA$^-$ Foxp3^{lo} population was made up of non-suppressive, non-Tregs.

In this study, we investigated the frequency of these three subpopulations in peripheral blood mononuclear cells (PBMCs) and tumor infiltrating lymphocytes (TILs) in lung cancer, and showed the accumulation of activated Tregs and also non-Tregs in the tumor microenvironment. We also examined the expression of CCR4 on these subpopulations and of chemokines in monocytes to clarify the mechanisms of Treg accumulation in lung cancer. Furthermore, we showed efficient Treg depletion by an anti-hCCR4 mAb (KM2760) and suggested its potential use in solid cancer patients.

MATERIALS AND METHODS

Patients and Clinical Samples

For preparation of a lung cancer tissue microarray (TMA), 384 specimens including 204 adenocarcinomas, 114 squamous cell carcinomas, 4 large cell carcinomas, 16 small cell carcinomas, 8 adenosquamous cell carcinomas and 4 others, and 34 metastatic tumors were used. Tumors were surgically removed from 384 patients who visited the Toyama University Hospital from December 1979 to May 2006. Some patients received chemotherapy or radiation therapy before surgery. For Treg analysis, PBMCs and tumor specimens were obtained from 20 patients with lung cancer who underwent surgery at Kawasaki Medical School Hospital from March 2012 to March 2014. For T-cell migration and proliferation analysis, PBMCs from three healthy donors were used. Peripheral blood or tumor specimens were obtained from healthy donors or patients after obtaining informed consent. These studies were approved by the ethics committee of Toyama University Hospital (IRB no. 19-12) and Kawasaki Medical School Hospital (IRB no. 603–6) and conducted in accordance with the Declaration of Helsinki.

Immunohistochemistry (IHC)

The TMA was prepared for two tumor nests in each sample punched out (core size, 0.6 mm) from formalin-fixed paraffin-embedded tumor tissues. For staining, a 4 μm thick section on a slide was used. To stain CCR4, a POTELIGEO TEST IHC (Kyowa Medex, Tokyo, Japan) was used. Briefly, after being deparaffinized, a tissue section was put in an oven for antigen retrieval for 40 minutes at 98°C. Endogenous peroxidase was blocked by adding 1 *N* HCl for 10 minutes. Mouse anti-hCCR4 mAb (KM2160; Kyowa Hakko Kirin, Tokyo, Japan) (1:200) was then added and incubated for 30 minutes. As a second antibody, a peroxidase-conjugated goat antimouse immunoglobulin (IgG) (1:1000) was added and incubated for 30 minutes. For staining CD4 and Foxp3, a rabbit anti-hCD4 mAb (clone EPR6855; abcam, Cambridge, UK) (1:100) and a mouse anti-hFoxp3 mAb (clone 236A/E7; abcam) (1:100), respectively, were added and incubated for 30 minutes. For doublestaining of CCR4 and CD4, a mouse/rabbit multiplex detection system (MP-001; Diagnostic Biosystems, Pleasanton, CA) was used. For staining of CCL17/TARC, goat anti-hCCL17/TARC (1:40) was used and incubated for 60 minutes. Simple stain MAX-PO (G) (414161; Nichirei, Tokyo, Japan) was used as a second antibody and incubated overnight. For staining of CCL22/MDC, a mouse anti-hCCL22/MDC mAb (clone 57226; R&D Systems, Minneapolis, MN) (1:50) was used and incubated overnight. For staining of CD163, a mouse anti-hCD163 mAb (clone 10D6; abcam) (1:1) was used and incubated for 30 minutes. As a second antibody, Envision Dual Link reagent (Dako, Glostrup, Denmark) was used and incubated for 30 minutes. Counterstaining was done with hematoxylin.

IHC Scoring of TMA

Interstitial cells and tumor cells were scored separately by the grade of distribution and intensity.[16] For grading distribution, 0 for 0%; 1 for 1 to 50%; and 2 for 51 to 100% were used. For grading intensity, 0 for no staining; 1 for weak staining; 2 for moderate staining, and 3 for marked staining were used. The mean of the sum of distribution and intensity scores from two distinct tumor TMA histospots was used as the definitive IHC score. Scores exceeding 2 (≥2.5) were defined positive. Scoring was performed by a pathologist.

Isolation of TILs

TILs were freshly isolated from lung cancer tissues using a Medimachine (BioLab, Osaka, Japan). Briefly, the tumor tissue was minced into pieces (<1 mm^3) and placed on a stainless steel screen with approximately 100 hexagonal holes, each surrounded by six microblades, in a sterile Medicon polyethylene chamber (BioLab) in 1 ml medium. A rotating screen brings the tissue into contact with the blades and it is homogenized. A Medicon with 50 μm separator screens was used. The procedure was repeated 3 times for 60 seconds at a constant speed of 100 rpm. Cells were collected after filtration using filters with a 50-μm pore size and then TILs were isolated.

Flow Cytometry

PBMCs and TILs were isolated by density gradient centrifugation using a Histo-Paque 1077 (Sigma–Aldrich, St. Louis, MO). Freshly isolated PBMCs or TILs were incubated with a mAb for 20 minutes at 4°C. The following mAbs were used: Anti-hCD3-V450 (clone UCHT1; BD Horizon, BD Bioscience, San Jose, CA), anti-hCD4-V500 (clone RPA-T4; BD Horizon), anti-hCD8-APC (clone RPA-T8; BD Pharmingen, BD Bioscience, San Jose, CA), anti-hCCR4-PerCP/Cy5.5 (clone 1G1; BD Pharmingen), anti-hFoxp3-Alexa Fluor 488 (clone 259D/C7; BD Pharmingen), and anti-hCD45RA-APC/H7 (clone HI100; BD Pharmingen). Intracellular Foxp3 staining was performed using a Human Foxp3 buffer set (BD Pharmingen) according to the manufacturer's instructions. With each sample, an isotype-matched control Ab was used to determine the positive and negative cell populations. Analysis was done by fluorescence activated cell sorting (FACS) Canto II.

CFSE Labeling

A carboxyfluorescein diacetate succinimidyl ester (CFSE) stock (10 mM in dimethyl sulfoxide (DMSO): Molecular Probes, Eugene, OR) stored at −30°C was thawed and diluted in phosphate buffered saline (PBS). The CD4 or CD8 T cells (5×10^6 cells/ml) in 0.1% bovine serum albumin

(BSA) PBS were incubated with 10 μM CFSE for 10 minutes at 37°C, diluted by five volumes of cold 0.1% BSA PBS, and kept on ice for 5 minutes. Cells were washed three times and used for experiments.

Cell Migration Assay

The cell migration was examined using EZ-TAXIScan (Effector Cell Institute, Tokyo, Japan) apparatus.[17,18] Two compartments of a cell migration assay chamber in etched silicon were connected by a 4 μm deep microchannel on a flat glass plate in the chamber. A glass coverslip was placed onto the glass plates. A reproducible chemoattractant gradient was formed in the microchannel without medium flow. The holder was filled with AIM V (Invitrogen, Carlsbad, CA) supplemented with 2.5% heat-inactivated pooled human serum and maintained at 37°C. $CD25^+$ CD4 T cells (1×10^5 cells in 1 μl) sorted from PBMCs which were left untreated or treated with anti-hCCR4 mAb (KM2760; Kyowa Hakko Kirin) using FACS Aria were injected into one compartment and 1 μl of CCL22/MDC (500 μg/ml; R&D Systems) solution into the other compartment. The migration of each cell in the channel was traced at time-lapse intervals using a charge coupled device (CCD) camera and recorded every 1 minute for 60 minutes. The cells that crossed a fixed gate were counted using a TAXIScan Analyzer (Effector Cell Institute).

To examine blocking activity of anti-hCCR4 mAb (KM2760) on migration, 24-well Transwell chemotaxis plates (3 μm pore size; Corning Costar, Corning, NY) were used. CD4 T cells (1×10^5) were placed in the upper chamber of a Transwell plate. Various concentrations of anti-hCCR4 mAb (KM2760) were added to both the upper and lower chambers. Then, CCL22/MDC (100 ng/ml) was added to the lower chamber and incubated for 4 hours at 37°C. After incubation, all cells in the lower chamber were collected and the number of cells was counted with an FACS Canto II.

Proliferation Assay

To obtain Tregs, a regulatory T-cell isolation Kit II (Miltenyi Biotec, Bergisch Gladbach, Germany) was used. $CD127^{dim/-}$ CD4 T cells were indirectly purified from PBMCs of healthy donors using biotin-conjugated antibodies against CD8, CD19, CD123, and CD127 with antibiotin antibody-coated magnetic beads. $CD25^+$ $CD127^{dim/-}$ CD4 Tregs were then purified and $CD25^-$ $CD127^{dim/-}$ CD4 T cells were used as control cells. $CD56^+$ NK cells, and CD4 and CD8 T cells were purified from PBMCs also using antibody-coated magnetic beads (Miltenyi Biotec). Tregs (1×10^4) and $CD56^+$ NK cells (1×10^4) were incubated overnight with or without anti-hCCR4 mAb (KM2760) at a concentration of 10 μg/ml in 96-well culture plates. The cells in the plates were washed three times and anti-hCD3/28 beads (Dynabeads Human T-Activator CD3/CD28, Invitrogen) were added to the culture and incubated for 8 hours for suppressor cell stimulation. CFSE-labeled responder cells (1×10^4/well) were then added and stimulated by anti-CD3/28 beads. After 24 hours, anti-CD3/28 beads were removed and the cells were kept cultured for another 3 to 4 days. After culture, the cells were harvested and CFSE dilution was analyzed with an FACS Canto II. The medium used was AIM V (Invitrogen) supplemented with 5% heat-inactivated pooled human serum, 2 mM L-glutamine, 100 IU/ml penicillin, and 100 μg/ml streptomycin.

RESULTS

Subpopulations of $Foxp3^+$ CD4 T Cells and Expression of CCR4 on Those Cells in PBMCs and TILs From Lung Cancer Patients

Subpopulations of $Foxp3^+$ CD4 T cells and expression of CCR4 on those cells in PBMCs and TILs from lung cancer patients were analyzed. The characteristics of 20 patients investigated are shown in Table 1. As shown in Figure 1, $Foxp3^+$ CD4 T cells were classified as three subpopulations: $CD45RA^+$ $Foxp3^{lo}$ resting/naive Tregs (Fr 1), $CD45RA^-$ $Foxp3^{hi}$ activated/effector Tregs (Fr 2), and $CD45RA^-$ $Foxp3^{lo}$ non-Tregs (Fr 3), as described by Miyara et al.[15] The mean ratios of resting/naive and activated/effector Tregs, and non-Tregs in CD4 T cells in PBMCs from 20 lung cancer patients were 0.6, 1.6, and 4.1%, respectively. However, the mean ratios of resting/naive and activated/effector Tregs, and non-Tregs in CD4 T cells in TILs were 0.5, 9.9, and 9.8%, respectively. The ratios of activated/effector Tregs and non-Tregs, but not resting/naive Tregs, in CD4 T cells in TILs were higher than those in PBMCs.

TABLE 1. Patient Characteristics ($n = 20$)

Characteristics	Patients	
Age, years		
Median	76.5	
Range	58–85	
≥65	16	80 (%)
Sex		
Male	17	85
Female	3	15
BMI (kg/m²)	22.6±2.6	
Smoking status		
Never	4	20
Former	13	65
Current	3	15
Pack-years	46.8±37.8	
FEV_1/FVC (%)	68.0±10.3	
FEV_1 % predicted	106.4±17.1	
Pathologic stage		
IA	6	30
IB	4	20
IIA	6	30
IIB	0	0
IIIA	4	20
Histology		
Adenocarcinoma	12	60
Squamous cell carcinoma	5	25
Large cell carcinoma	2	10
Adenosquamous cell carcinoma	1	5

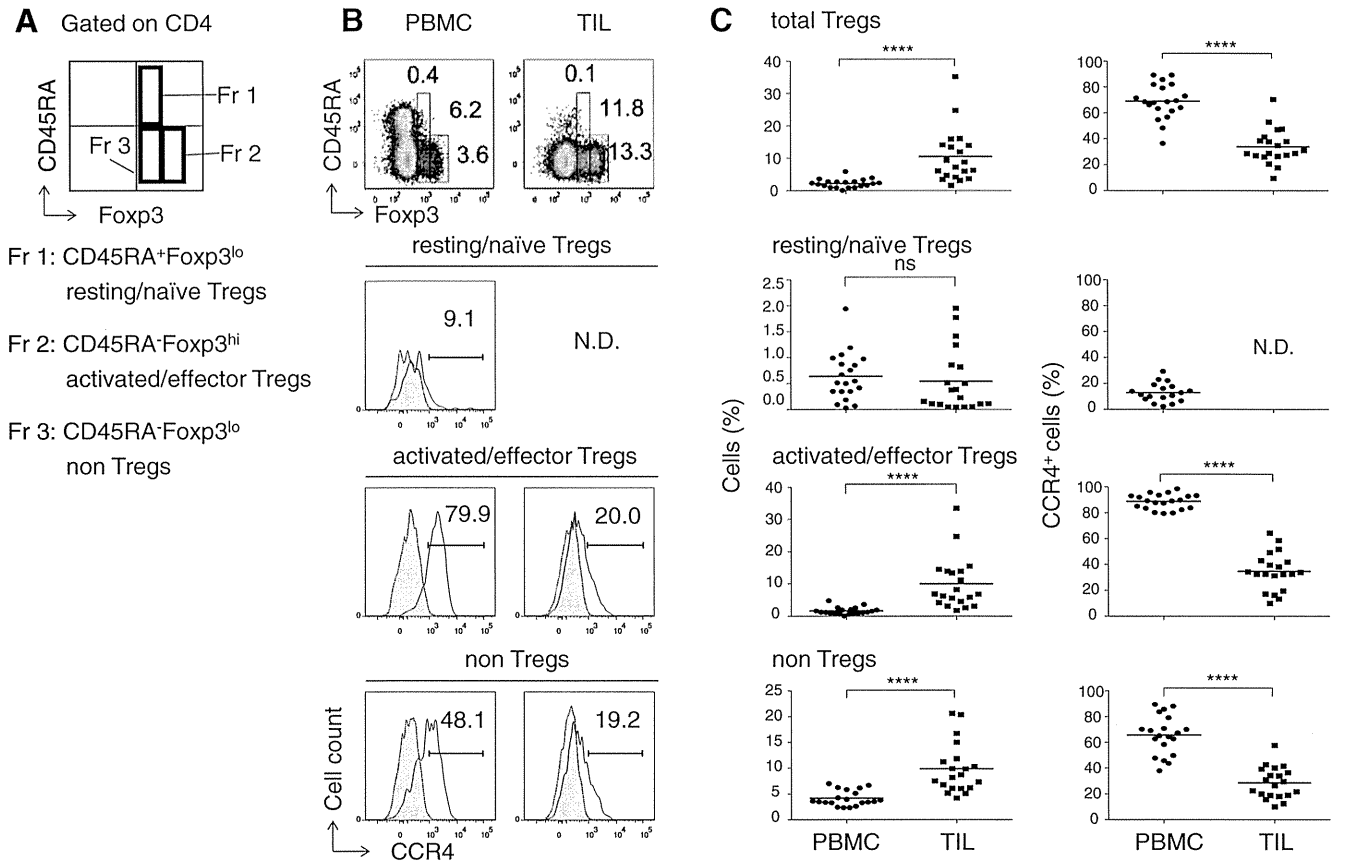

FIGURE 1. Analysis of subpopulations of Foxp3⁺ CD4 T cells and expression of CCR4 on those cells in PBMCs and TILs from lung cancer patients. *A*, classification of Foxp3⁺ CD4 T cells as CD45RA⁺ Foxp3^{lo} resting/naive Tregs (Fr 1), CD45RA⁻ Foxp3^{hi} activated/effector Tregs (Fr 2) and CD45RA⁻ Foxp3^{lo} non-Tregs (Fr 3). *B*, representative dot plots showing subpopulations of Foxp3⁺ CD4 T cells in PBMCs and TILs and histograms showing the CCR4 expression on those cells using anti-hCCR4 mAb (1G1) and the isotype-mached control Ab (gray). Figures indicate % positive cells. *C*, ratios of resting/naive and activated/effector Tregs, and non-Tregs in CD4 T cells (left panel) and CCR4 expression on those cells (right panel) in PBMCs and TILs from 20 lung cancer patients. Horizontal bar, mean value. Statistical analysis was done by the Mann-Whitney *U* test (**** $p < 0.0001$). Each dot indicates a single patient.

The CCR4 expression on those populations was then determined. The mean ratios of CCR4⁺ cells in resting/naive and activated/effector Tregs, and non-Tregs in PBMCs were 13.0, 88.7, and 65.6%, respectively. However, the mean ratios of CCR4⁺ cells in activated/effector Tregs and non-Tregs in TILs were 34.6 and 28.5%, respectively. Insufficient resting/naive Tregs were available for the analysis in TILs. The ratios of CCR4⁺ cells in activated/effector Tregs and non-Tregs in TILs were lower than those in PBMCs.

Detection of CCR4- and CCL22/MDC-Expressing Cells in Lung Cancer by IHC Using a TMA

CCR4-, CCL17/TARC-, and CCL22/MDC-expressing cells in lung cancer were analyzed by IHC using TMA. For evaluation, the staining score was determined by the sum of scores of distribution and intensity (See Materials and Methods Section). Two TMA spots were examined in each sample and the mean score was calculated for the definitive score. A definitive score exceeding 2 (≥2.5) was defined as positive. As shown in Figure 2*A* and *B*, CCR4-expressing stroma infiltrating lymphocytes were detected in 78 (20.3%) of 384 samples and CCR4-expressing tumor cells were detected in only 1 (0.3%). CCL17/TARC-expressing stroma infiltrating monocytes were detected in 5 (1.3%) of 384 samples and CCL17/TARC-expressing tumor cells were detected in 2 (0.5%). CCL22/MDC-expressing stroma infiltrating monocytes were detected in 117 (30.5%) of 384 samples and CCL22/MDC-expressing tumor cells were detected in none. As shown in Figure 3*A*, CCR4-stained lymphocytes were mostly CD4 and some of those cells were also positive for Foxp3. As shown in Figure 3*B*, some CCL22/MDC-expressing cells were likely to be CD163-positive M2 macrophages. CCR4 expression was correlated with CCL22/MDC (Figure 3*C*).

By enzyme-linked immunosorbent assay using plasma and malignant pleural effusion, we detected a significant amount of CCL17/TARC in 1 patient and CCL22/MDC in several patients out of a total 17 lung cancer patients in a separate analysis (data not shown). Predominance of CCL22/MDC compared with CCL17/TARC in lung cancer was consistent with the IHC results.

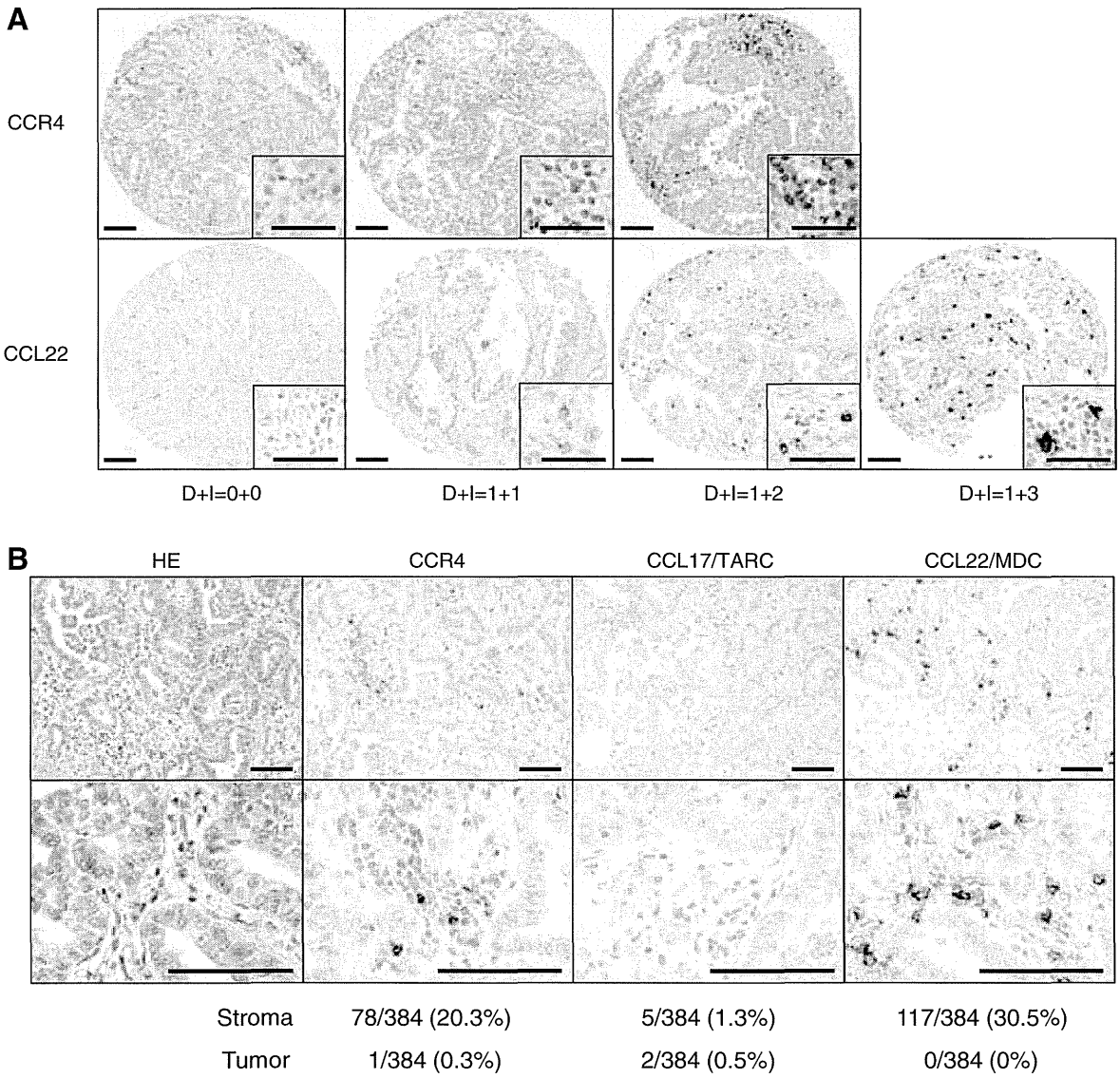

FIGURE 2. Analysis of CCR4-, CCL17/TARC- and CCL22/MDC-expressing cells in lung cancer by Immunohistochemistry (IHC) using a tissue microarray (TMA). *A*, staining score was determined by a sum of scores of distribution (D) and intensity (I) (See Materials and Methods Section). Representative intensity (I) scoring with density (D) score 1 for CCR4 and CCL22 are shown. Two TMA spots were examined in each sample and the mean score was calculated for the definitive score. A definitive score exceeding 2 (≥2.5) was considered positive. Scale bar denotes 100 μm for low magnification and 50 μm for high magnification (inset). *B*, representative staining of TMA with CCR4 (score 3), CCL17/TARC (score 0) and CCL22/MDC (score 3) and the number of positive samples for stroma-infiltrating cells and tumor cells in the total of 384 samples are shown. HE, hematoxylin/eosin. Scale bar denotes 100 μm.

Efficient migration of a CCR4$^+$CD25$^+$ CD4 T-cell population in PBMCs to the CCL22/MDC gradient and elimination of migrating cells by adding an anti-hCCR4 mAb (KM2760) to the culture

Antihuman (h) CCR4 mAb (KM2760) is a defucosylated antibody developed by the Potelligent technology and it has been shown to exert antibody-dependent cellular-cytotoxicity (ADCC) against CCR4-expressing cells by using NK cells as effector cells.[19] We examined the migration of CD25$^+$ CD4 T cells sorted from PBMCs which were left untreated or treated with anti-hCCR4 mAb (KM2760) to the CCL22/MDC gradient using EZ-TAXIScan apparatus. Expression of CCR4 on sorted cells was confirmed with an FACS Canto II (data not shown). As positive and negative controls for migration, CCR4$^+$ CD4 T cells and CCR4$^-$ CD4 T cells sorted from anti-hCCR4 mAb (1G1) (with no ADCC activity) and anti-hCD4 mAb-treated PBMCs were used. As shown in Figure 4, efficient migration to the CCL22/MDC gradient was observed in a CD25$^+$ CD4 T-cell population sorted from anti-hCCR4 mAb (KM2760)-untreated PBMCs. Migrating cells were markedly diminished in a CD25$^+$ CD4 T-cell population sorted from anti-hCCR4 mAb (KM2760)-treated PBMCs.

We further examined whether an anti-hCCR4 mAb (KM2760) could directly block the migration of CD4 T cells

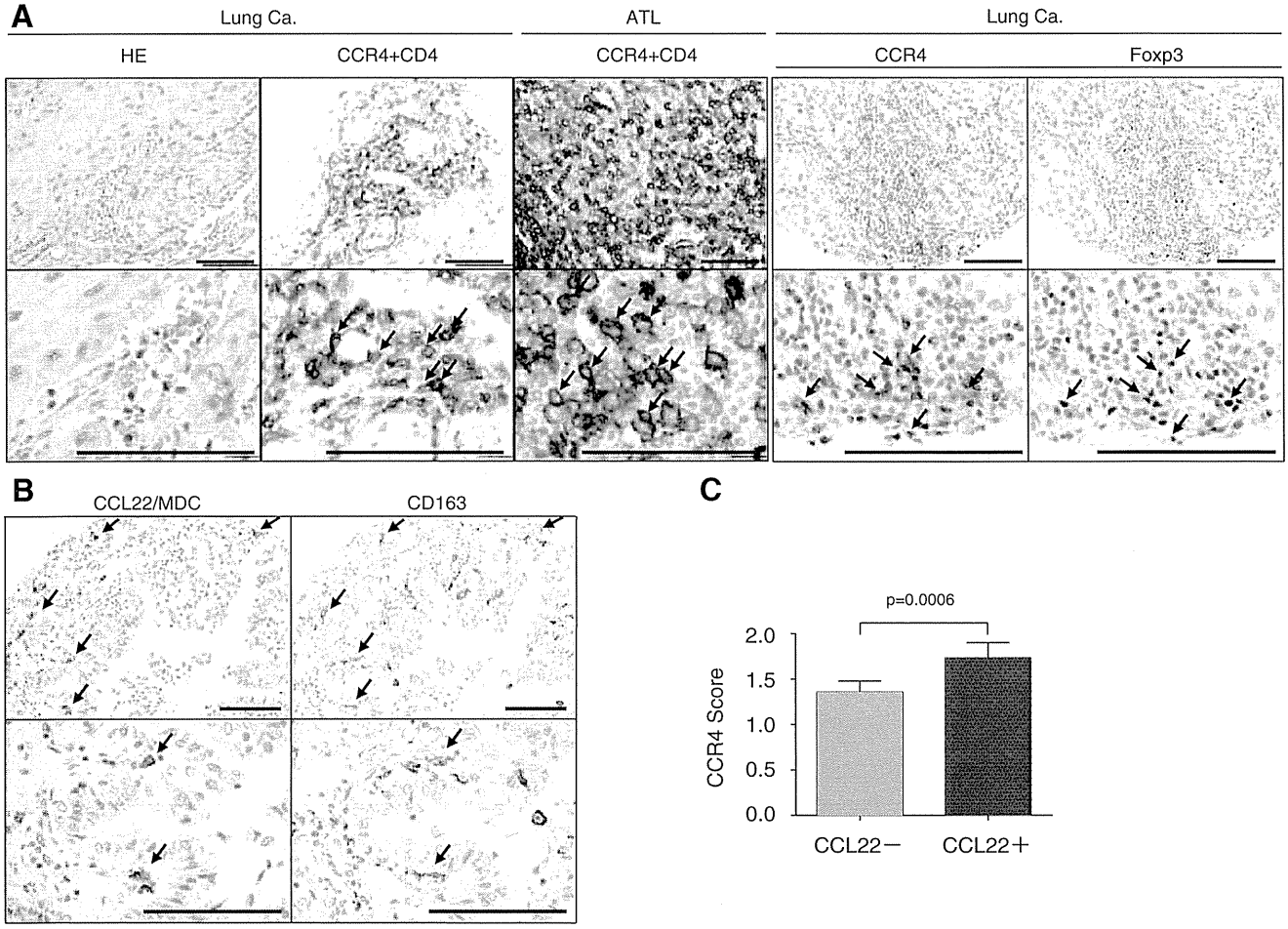

FIGURE 3. *A,* Immunohistochemistry (IHC) staining of tissue microarray (TMA) with anti-CCR4, anti-CD4, and anti-Foxp3 in lung cancer tissue. In double staining of CCR4 and CD4, CCR4 is stained brown and CD4 is stained red. Arrows indicate double-stained cells. ATL is a positive control. Staining of CCR4 and Foxp3 are done on serial sections. Arrows show the cells stained with either mAb. Scale bar denotes 100 μm. *B,* IHC staining of serial sections with anti-CCL22 and anti-CD163. Arrows show the cells stained with either mAb. *C,* Correlation of CCR4 with CCL22 score. $CCL22^-$ (score 0–2): $n = 267$, $CCL22^+$ (score ≥ 2.5): $n = 117$. CCR4 score is the mean value with the error bar showing 95% confidence interval. Statistical analysis was done by the Mann-Whitney *U* test.

to the CCL22/MDC gradient without NK cells using Transwell plates. As shown in Figure 4*C*, anti-hCCR4 mAb (KM2760) had no blocking effect on migration of CD4 T cells or any Treg population in a range of antibody concentrations.

Inhibition of CD3/CD28-mediated proliferative response of CD4 and CD8 T cells by $CD25^+$ CD4 Tregs and abrogation of inhibition by treatment with an anti-hCCR4 mAb (KM2760)

We then examined inhibition of CD4 and CD8 T-cell proliferation by Tregs and abrogation of inhibition by the treatment of Tregs with an anti-hCCR4 mAb (KM2760). $CD127^{dim/-}$ CD4 T cells were indirectly purified from PBMCs of healthy donors using biotin-conjugated antibodies against CD8, CD19, CD123, and CD127 with antibiotin antibody-coated magnetic beads. $CD25^+$ $CD127^{dim/-}$ CD4 Tregs were then purified and $CD25^-$ $CD127^{dim/-}$ CD4 T cells were used as control cells. $CD56^+$ NK cells, and CD4 and CD8 T cells were purified from PBMCs also using antibody-coated magnetic beads. Tregs (1×10^4) and $CD56^+$ NK cells (1×10^4) were incubated overnight with or without anti-hCCR4 mAb (KM2760) at a concentration of 10 μg/ml in 96-well culture plates. After washing the cells in the plates, anti-CD3/CD28 beads were added. The CFSE-labeled responder CD4 and CD8 T cells were then added and proliferation was determined after 5 to 6 days. As shown in Figure 5, proliferation of either CD4 or CD8 T cells stimulated by anti-CD3/CD28 beads was inhibited by culturing with $CD25^+$ $CD127^{dim/-}$ CD4 Tregs and $CD56^+$ NK cells without anti-hCCR4 mAb (KM2760). The inhibition was abrogated in the culture with an anti-hCCR4 mAb (KM2760).

DISCUSSION

$Foxp3^+$ CD4 T cells were composed of three distinct populations and classified according to the expression of CD45RA and Foxp3 on those cells.[15] In this study, we showed that the ratios of activated/effector Tregs and non-Tregs in $Foxp3^+$ CD4 T cells were higher in TILs obtained from surgically removed specimens than those in PBMCs in lung cancer patients. The

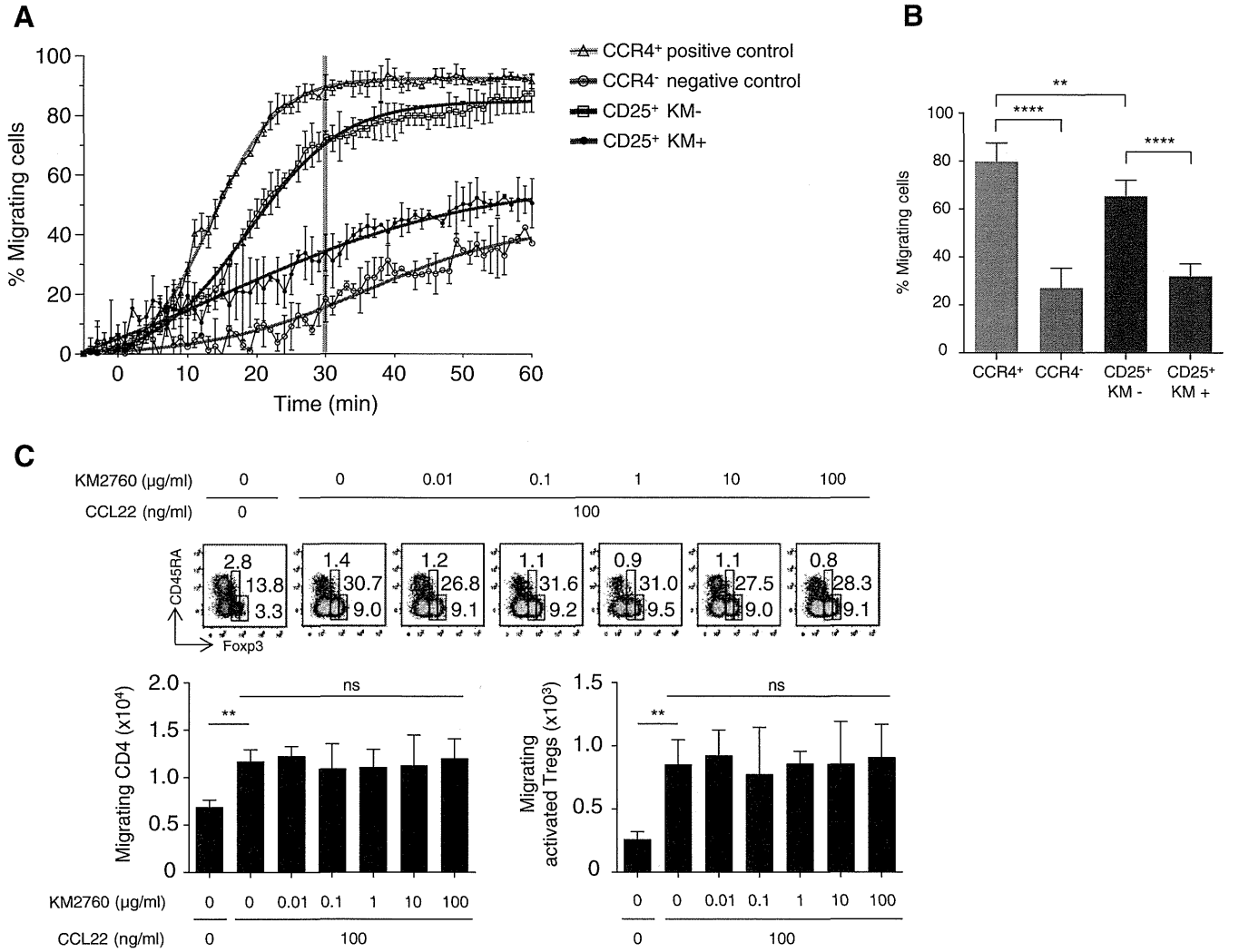

FIGURE 4. Efficient migration of a CCR4$^+$ CD25$^+$ CD4 T cell population in PBMCs to the CCL22/MDC gradient and elimination of migrating cells by adding an anti-CCR4 (KM2760) mAb to the culture. *A*, migration of CD25$^+$ CD4 T cells (CD25$^+$KM$^-$ and CD25$^+$KM$^+$) sorted from PBMCs which were left untreated or treated with anti-hCCR4 mAb (KM2760), respectively, using FACS Aria to the CCL22/MDC gradient was investigated using EZ-TAXIScan apparatus. CCR4$^+$ CD4 T cells and the CCR4$^-$ CD4 T cells sorted from anti-hCCR4 (1G1) mAb (without ADCC activity) and anti-hCD4 mAb-treated PBMCs were used as positive and negative controls, respectively, for migration. The results are the mean ± SD of duplicates. *B*, the % migrating cells to CCL22/MDC counted at 30 minutes in the assay. The results are the mean ± SD of three individuals. Statistical analysis was done by Welch's *t* test (** $p < 0.01$, **** $p < 0.0001$). *C*, blocking of Treg migration by an anti-hCCR4 (KM2760) mAb. Purified CD4 T cells (1×10^5) were placed in the upper chambers and CCL22 (100 ng/ml) was placed in the lower chambers of Transwell plates. A different amount of anti-hCCR4 (KM2760) mAb was present in the upper and lower chambers during the migration assay. After incubation for 4 hours, all cells in the lower chambers were collected and the number of cells was counted with a FACS Canto II. FACS dot plots showed subpopulations of Foxp3$^+$ CD4 T cells (top). Numbers in the dot plot panel denote % of resting/naive Tregs, non-Tregs and activated/effector Tregs in the migrated Foxp3$^+$ CD4 T cells from top to bottom. Migration of non-Tregs and activated/effector Tregs to CCL22/MDC was observed, but no blocking of migration by addition of KM2760 was observed. Numbers of migrating CD4 T cells (bottom left) and activated/effector Tregs (bottom right) are shown. The results are the mean ± SD of triplicate experiments. Statistical analysis was done by the Welch's *t* test for two groups and by ANOVA for multiple groups (** $p < 0.01$). No blocking of migration was observed.

findings suggested that the activated/effector Tregs and also non Tregs appeared to accumulate in the tumor from PBMCs. No increase in resting/naive Tregs in TILs suggests conversion from resting/naive Tregs to activated/effector Tregs in the tumor as described previously.[15,20] The non Treg population contains Th2 and Th17 that could be involved in effector mechanisms in tumors.[1,15] In our analysis of TILs from 11 lung cancer patients, CD45RA$^-$ Foxp3^{lo}, a non Treg population contained CRTH2 (CD294)-positive Th2 cells (approximately 9%) and CCR6-positive Th17 cells (approximately 14%), although the rest of cells were not clearly analyzed. Miyara et al. reported detection of transcription factor RAR-related orphan receptor C (RORC) and secretion of IL-17, and also secretion of interferon gamma (IFNγ) in stimulation with PMA/ionomycin with the cells in